Space Sci Rev (2013) 176:177–215
DOI 10.1007/s11214-011-9835-3

The Heliospheric Magnetic Field

André Balogh · Géza Erdõs

Received: 12 July 2011 / Accepted: 16 September 2011 / Published online: 18 October 2011

Abstract The Heliospheric Magnetic Field (HMF) is the physical framework in which energetic particles and cosmic rays propagate. Changes in the large scale structure of the magnetic field lead to short- and long term changes in cosmic ray intensities, in particular in anti-phase with solar activity. The origin of the HMF in the corona is well understood and inner heliospheric observations can generally be linked to their coronal sources. The structure of heliospheric magnetic polarities and the heliospheric current sheet separating the dominant solar polarities are reviewed here over longer than a solar cycle, using the three dimensional heliospheric observations by Ulysses. The dynamics of the HMF around solar minimum activity is reviewed and the development of stream interaction regions following the stable flow patterns of fast and slow solar wind in the inner heliosphere is described. The complex dynamics that affects the evolution of the stream interaction regions leads to a more chaotic structure of the HMF in the outer heliosphere is described and discussed on the basis of the Voyager observations. Around solar maximum, solar activity is dominated by frequent transients, resulting in the interplanetary counterparts of Coronal Mass Ejections (ICMEs). These produce a complex aperiodic pattern of structures in the inner heliosphere, at all heliolatitudes. These structures continue to interact and evolve as they travel to the outer heliosphere. However, linking the observations in the inner and outer heliospheres is possible in the case of the largest solar transients that, despite their evolutions, remain recognizably large structures and lead to the formation of Merged Interaction Regions (MIRs) that may well form a quasi-spherical, "global" shell of enhanced magnetic fields around the Sun at large distances. For the transport of energetic particles and cosmic rays, the fluctuations in the magnetic field and their description in alternative turbulent models remains a very important research topic. These are also briefly reviewed in this paper.

Keywords Heliosphere · Magnetic fields · Solar wind · Magnetic fluctuations · Energetic particle transport

A. Balogh (✉)
The Blackett Laboratory, Imperial College London, London, UK
e-mail: balogh@issibern.ch

G. Erdõs
Research Institute for Particle and Nuclear Physics (KFKI RMKI), Budapest, Hungary

1 Introduction

There have been several detailed reviews of the Heliospheric Magnetic Field (HMF) in recent years (see, e.g., Smith 2007; Zurbuchen 2007; Balogh and Jokipii 2009 and references therein). Several key space missions since the 1960s have provided a large number of observations in the heliosphere, although not a comprehensive coverage throughout its volume or its boundaries. Given that the magnetic field in space can only be measured in situ, the observations are limited to the trajectories of the space probes themselves. Given also the variability of the HMF as a function of the solar activity cycle, the temporal coverage versus the spatial coverage has introduced some limitations which make a general, time-dependent description or model of the HMF incomplete in its details. The observations have allowed some (successful) testing of the basic model of Parker (1959) and a description which provides a realistic framework for discussing the effects of the HMF on the propagation of cosmic rays in the heliosphere. The Parker spiral model of the HMF, in its three-dimensional form (for a comprehensive description, see Smith 2007), is a consequence of the solar wind flowing radially at a constant speed from the Sun which carries the magnetic field lines. Despite the assumptions of the model, it has proved to be a good first approximation and has provided the basic framework (or coordinate system) in which the temporal and spatial variabilities can be described. Although some potentially important effects have been proposed that could in principle alter the large scale geometry of the HMF (e.g. Jokipii and Kóta 1989; Fisk 1996), these effects may contribute in a temporary or locally restricted way and cannot be considered to alter the basic Parker model significantly.

Long-term assessments of the distribution of the magnetic field direction as a function of heliocentric distance and heliolatitude have been carried out by, e.g., Thomas and Smith (1980), Forsyth et al. (2002). These confirm the generally Parker-spiral configuration of the direction of the HMF, with a relatively wide, quasi-Gaussian distribution around the mean Parker angle. Recently, Borovsky (2010) examined in detail the variations of the magnetic field directions around the nominal Parker angle in the inner heliosphere and found multiple causes for systematic deviations that are observed outside the Gaussian distributions. Of these, intervals which contain remnants of Coronal Mass Ejections appear to dominate, although there are also other, generally unexplained intervals when the magnetic field remains nearly radial for extended intervals (several hours, up to a day). Long duration radial magnetic field intervals have been reported by Jones et al. (1998) and Wang et al. (2003) at heliocentric distances less than 10 AU. If not associated with coronal ejecta, these intervals may be due to a sudden drop in solar wind speed close to the Sun which introduces a kink in the magnetic field that stretches out as the solar wind propagates away from the Sun (see Gosling and Skoug 2002). Wang et al. (2003) have proposed a similar model in which a long duration low-speed plateau in the solar wind speed near the Sun can generate (at least qualitatively) the observed radially oriented magnetic field.

Magnetic field measurements on the Mariner 2 mission to Venus were the first, in 1962, to chart the magnetic field between 1 and 0.72 AU. A decade later, Mariner 10 also provided a set of magnetic field data between its second and third encounters with Mercury in 1973–1974 to 0.46 AU. Observations from the early missions, together with their heliospheric coverage, were reviewed by Behannon (1978). The coverage in heliocentric distance and heliolatitude of the space missions that have contributed most critically to our knowledge of the HMF are shown in Fig. 1. The region from 0.3 to 1 AU in the ecliptic plane was investigated by the two Helios probes in the 1970s and 1980s. Pioneers 10 and 11 were the first to reach out to the distance of Saturn (10 AU) in the ecliptic plane. Voyagers 1 and 2, following their planetary encounters (all near the ecliptic), continued into the outer heliosphere

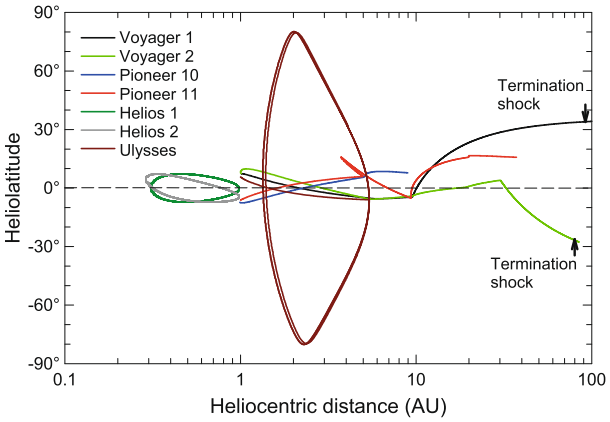

Fig. 1 Heliospheric trajectories of seven key missions that have provided extensive observations of the HMF (in addition to those spacecraft that have remained at 1 AU). The location of the Termination Shock when the two Voyager spacecraft first encountered it is also indicated

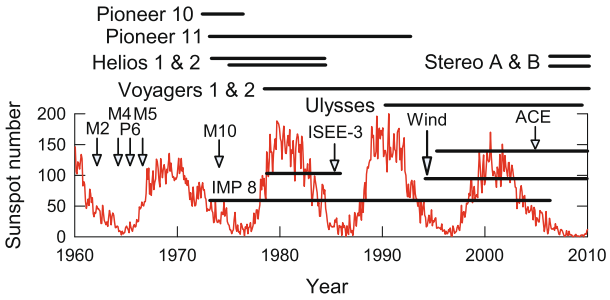

Fig. 2 Selected heliospheric missions in the context of the solar activity cycles since 1960. Early missions are indicated by arrows: Mariners 4, 5 and 10 (M4, M5, M10) and Pioneer 6 (P6); these missions generally provided short (a few months long) data sets, but provided early insights into the solar wind and the interplanetary magnetic field. IMP 8, ISSE-3, Wind and ACE have been the key monitors of the HMF at 1 AU. The scientific operation of Pioneer 10 in fact extended to 1996, but the magnetometer stopped operating in late 1975

and encountered the first outer boundary of the heliosphere, the termination shock, at 94 AU and 84 AU, respectively. Both Voyager probes departed from the ecliptic plane after their planetary flybys and explored the mid-heliolatitude outer heliosphere, respectively, in the northern and southern hemispheres. The Ulysses probe has been the only mission to explore the HMF at high heliolatitudes, including the polar heliosphere, at heliocentric distances between 1.3 and 5.5 AU. These missions covered more than three solar activity cycles, as illustrated in Fig. 2.

In addition, a large number of Earth-orbiting satellites and probes in orbits near 1 AU have provided key data on the structure and on the dependence of the HMF on the phase of the solar activity cycle. Most notable among the many Earth-orbiting spacecraft that served as a monitors of solar wind and heliospheric magnetic field conditions at 1 AU was IMP-8, operating from 1973 to 2006 in a near-circular, 35 Earth radii orbit, spending 7 or 8 days in the solar wind each 12.5 day orbit. The ISEE-3 and ACE spacecraft in orbit around the L1 Lagrange point of the Sun-Earth system provided many years of continuous high quality magnetic field measurements. ACE, launched in 1995, remains on station to continue the provision of reference solar wind and magnetic field measurements. The Wind spacecraft, launched in 1994, has a complex orbit history: using multiple lunar swing-bys it has repeat-

edly explored the region upstream of the Earth's magnetosphere, out to the Lagrange point L1 and remains fully operational for magnetic field and solar wind measurements. NASA's OMNI data set, generated from the many spacecraft that have made solar wind and magnetic field measurements in the near-Earth interplanetary space, provides a high quality reference data set from 1963 to today.

The two Stereo spacecraft were launched in 2006 into Earth-like heliocentric orbits. One of the spacecraft ("Ahead") is slightly closer to the Sun, hence its heliographic longitude is westward from the Earth, evolving at a rate of ∼22°/year. The second ("Behind") is at a slightly larger heliocentric orbit, thus has a longer than 1 year period, and is progressing eastward from the Earth at the same annual rate. These spacecraft are particularly well placed to study the dynamic evolution of solar wind and magnetic field structures in heliographic longitude.

In Sect. 2, we shall describe the origin of the HMF and its relationship to magnetic fields in the corona; progress in relating coronal magnetic fields to the observed HMF was made possible by the Ulysses mission which provided the three-dimensional observations that have led to a now well-established view of the fundamentally two-regimes description of the solar wind and its consequences for the structure and dynamics of the HMF. The signature of the Sun's magnetic polarity reversal at solar maximum in the HMF is also described. In Sect. 3, we describe the structures of the magnetic field around solar minimum, when the three dimensional heliosphere is relatively simple. Fast solar wind from the dominant polar coronal holes fills much of the volume of the heliosphere. The wind speed there is generally high and relatively uniform, as is the unipolar magnetic field. As discovered by Ulysses, the magnetic flux density in the fast wind is independent of heliolatitude, but, as shown in Sect. 3, the reduction in the solar magnetic field between the minima in solar cycles 22 and 23 are reflected in the heliospheric magnetic flux density. In the equatorial region, there is a band of slow solar wind around the Sun's magnetic equator which extends into space as the Heliospheric Current Sheet. As the HCS is inclined to the solar equator, a near-equatorial observer in space will be immersed in a succession of fast and slow solar wind streams. As the fast wind follows and catches up with the preceding slow wind stream, the interaction leads to a quasi-stationary pattern of dynamic regions, the Corotating Interaction Regions. These dominate the dynamics of the magnetic field out to beyond 10 AU. The interactions at greater heliocentric distances lead to a complex mixing of the remnants of interaction regions, leading to a chaotic structure of the magnetic field in the outer heliosphere. Around solar maximum, solar transients dominate the heliosphere. In Sect. 4, Coronal Mass Ejections (CMEs) and their interplanetary counterparts, ICMEs, are described in some detail. These are distributed over all heliolatitudes so that the heliosphere is significantly filled with hot coronal material and with the remnants of coronal structures, particularly in the form of twisted coronal loops which may remain attached to the corona as they expand, to form large scale (∼0.4 AU in diameter at 1 AU) magnetic flux ropes. Considerable progress has been made in modelling these by a range of techniques, but knowledge of their three dimensional structure and extent remain subject to observational limitations. However, as the most important component in the heliospheric magnetic field for several years around solar maximum, they play a very important role in the propagation and modulation of cosmic rays, so understanding their large scale structure, evolution and dynamics is a key to progress in cosmic ray studies. The fundamentally chaotic nature of the HMF in the outer heliosphere arises from the continuing dynamic interactions that stir the solar wind as it propagates towards the heliospheric Termination Shock (TS) at ∼90 AU. The propagation of energetic particles in the Heliospheric Magnetic Field is briefly addressed in Sect. 5. The complex turbulence phenomena observed in the heliosphere remain to be fully understood.

It now seems clear that the turbulence is fundamentally quasi-two dimensional, with a relatively smaller power in the fluctuations along the magnetic field than perpendicular to it. This division helps explain the discrepancy between calculated and observed transport coefficients, as reviewed in Sect. 5. For comparison with the observations, the heliographic dependences of the transport coefficients are investigated, using the quasi-linear theory of particle transport as the baseline. In Sect. 6, a brief and non-exhaustive list of outstanding questions concerning the Heliospheric Magnetic Field serves as a summary to this review.

2 The Origin of the Heliospheric Magnetic Field

In Parker's (1959) original model, the magnetic field in the corona is uniform and radial as is the flow of the solar wind. The solar corona is known to be very non-uniform, generally highly structured, with most of the magnetic field observed at the photosphere in closed loops so that there are no open magnetic field lines that could be taken by the accelerating solar wind and carried into the heliosphere. However, parts of the corona appear to be open, without loop structures that would retain the solar magnetic field. Coronal holes are known to be the origin of the fast solar wind. The acceleration of the slow wind remains controversial, although its properties imply origins that point to the magnetically closed corona. The magnetic field measured in the heliosphere generally originates in the open magnetic flux of the Sun (Wang 2009). The exception when the magnetic field lines remain attached at both ends in the corona or perhaps form closed loops arises as a consequence of Coronal Mass Ejections. Magnetic fields in the slow solar wind originate in previously closed structures that open up as part of the process of the acceleration of the slow solar wind itself.

Modelling the solar corona by making the assumption that it is current-free, and using the measured photospheric magnetic field as an inner boundary condition has proved to be a successful method for determining the distribution of the magnetic field on a virtual spherical surface at about 2.5 solar radii. This method, the Potential Field Source Surface (PFSS) model (see Hoeksema 1989 and references therein) has provided consistent maps of the source surface field contours since 1976. A critical assessment of the method, with refinements to overcome the problem of the line of sight measurements of the photospheric magnetic field was presented by Wang and Sheeley (1992). The technique has in fact been proven to be quite successful in relating interplanetary observations to the coronal origin of the solar wind. The PFSS model has also been used to generate coronal field models, based on a modelled evolution of the photospheric magnetic field through the solar cycle (Wang and Sheeley 2003).

The source surface magnetic field can be expanded into a series of dipole, quadrupole and octupole terms. At solar minimum, the magnetic field can be represented by a dominant dipole term with its axis coinciding with the Sun's rotation axis. At the approach of solar activity maximum, the axial dipole term no longer dominates and the source surface magnetic field is better described by the quadrupolar (and higher order) terms. However, an alternative modelling can represent the magnetic field by that of a dipole whose axis is rotating in the Sun's meridional plane; this model has the conceptual advantage of providing a representation for the magnetic polarity reversal of the Sun near solar maximum. Such a model of the rotating solar dipole is shown in Fig. 3, derived by using the photospheric magnetic field measurements and applying the PFSS model to the observations. The reversal of the magnetic field as observed by Ulysses in 2000 (Jones et al. 2003) at the last solar maximum, was somewhat more complex, but in essence backing up the model shown in Fig. 3. We note that if higher order (quadrupole) terms are used in the model, which are an equivalent

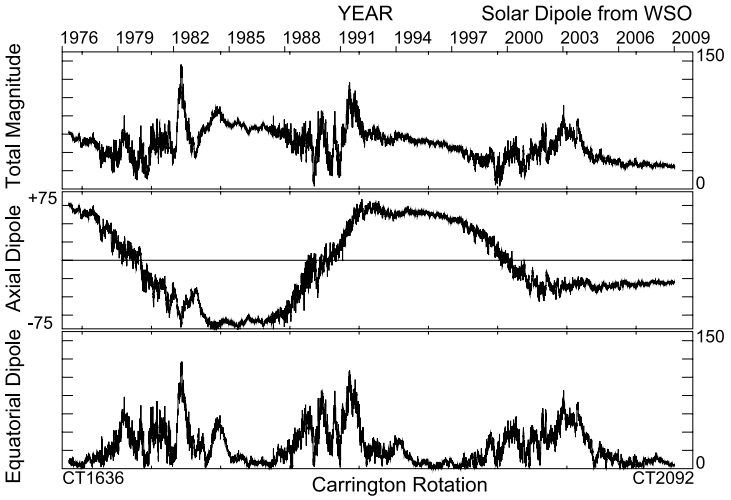

Fig. 3 Modelling of the solar magnetic field using a combination of an axial and an equatorial dipole. During the years around solar minimum. the axial dipole dominates the total field, but around solar activity maximum it decreases and changes sign, corresponding to the polarity reversal of the Sun's magnetic field. During the reversal process, the equatorial dipole increases in strength. A combination of the two dipoles can be interpreted as a dipole rotating in the Sun's meridional plane during the polarity reversal. (Courtesy of J. Todd Hoeksema, Wilcox Solar Observatory, Stanford University)

to the equatorial dipole presented in Fig. 3, a more physically representative model of the magnetic reversal process is obtained (Wang et al. 2002a).

As illustrated in Fig. 4, the PFSS model of the magnetic field represents the areas of the two magnetic polarities on the source surface, separated by the magnetic neutral line that corresponds to the magnetic equator of the Sun. Close to solar minimum, the dominance of the axial dipole leads to a neutral line close to the solar equator. When the dipole is not completely axial, the magnetic equator, in projection, becomes a wavy line, with the north-south maximum excursion corresponding to the extent of the dipole tilt. Another interpretation of a wavy neutral line is to retain the axial dipole term, but complement it either with an equatorial dipole (as in Fig. 3) or with a quadrupole term (that can often be attributed to the contribution of active regions). In fact, in the upper panel of Fig. 4 the neutral line appears to cross the solar equator four times; this implies the contribution of a quadrupole term in the source surface magnetic field. Around solar maximum activity, near the polarity reversal, the decay of the axial dipole and the increase in the non-axial terms make the projection of the magnetic polarities on the source surface more complex and the neutral line can become in fact topologically disconnected. This is considered to be an artefact, as the measurement of photospheric magnetic fields at heliolatitudes greater than $\sim 70^\circ$ has large uncertainties and the polar fields affect the accuracy of the PFSS model in the polar regions. The magnetic neutral line is in fact the source surface trace of the Heliospheric Current Sheet that extends throughout the heliosphere and separates magnetic fields of positive and negative polarities (Schulz 1973; Thomas and Smith 1981; Smith 2001).

Magnetic field observations onboard spacecraft provide the value of the magnetic field embedded in the solar wind flow. Although the radial flow and the rotation of the Sun twist the magnetic field lines into the Parker spiral, the field retains, on average, the polarity of the field from the location on the source surface from which solar wind stream that carries

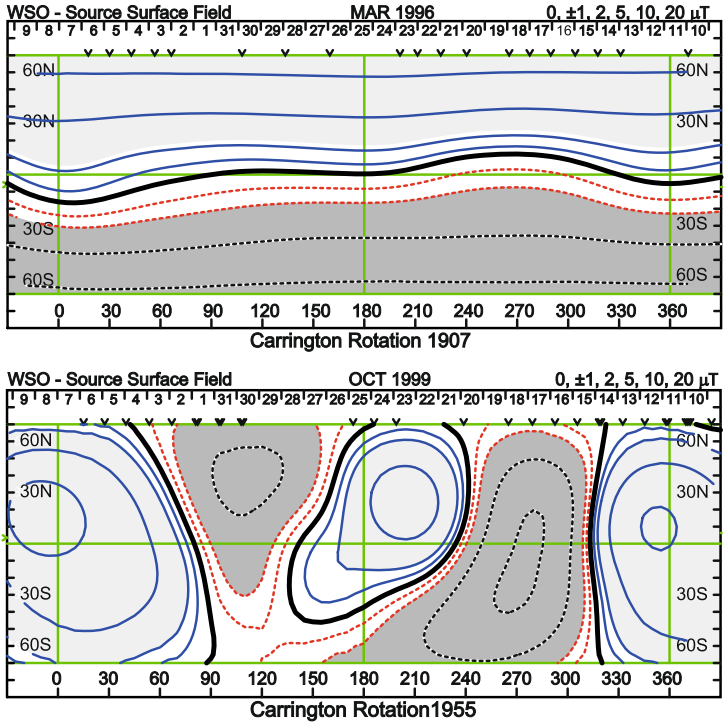

Fig. 4 Computed coronal magnetic field maps, using the potential field, source surface technique, for a Carrington rotation near solar minimum (*upper panel*) and near solar maximum (*lower panel*). The Sun's magnetic equator, the coronal neutral line (*thick black line*) is close to the solar equator at solar minimum, separating the two hemispheres of uniform and opposite polarity. Near solar maximum, the Sun's dipole moment is much weaker and its axis is close to the solar equatorial plane, resulting in a much more complex neutral line separating the two opposite polarities. Important contributions from the quadrupole and octupole magnetic moments further complicate the calculated magnetic field contours on the source surface (from Balogh 2002, data by courtesy of J. Todd Hoeksema, Wilcox Solar Observatory, Stanford University)

it originates. For a nearly stationary observer (on the timescale of the solar rotation), the observed polarity therefore should correspond to the polarity at the location where the solar wind can be mapped back onto the source surface. Observations by spacecraft close to the solar equator (in Earth orbit or at the L1 point) usually sample the polarities on both sides of the solar magnetic neutral line, leading to the well established sector pattern (Wilcox and Ness 1965; Schulz 1973). The pattern can be quite stable over a series of Carrington Rotations around solar minimum when the magnetic fields evolve slowly on the Sun, but becomes more variable when solar activity is at a high level. In quiet times, in the ecliptic plane, there are two or four magnetic sectors in each solar rotation, depending on the waviness of the near-equatorial magnetic neutral line.

The measured magnetic polarities at 1 AU from 1976 to 1994 were compared to the modelled or predicted polarities based on two different methods by Wang and Sheeley (1995). Their objective in fact was to determine the nature of the correction that had to be applied to the raw photospheric magnetic measurements to match the sector structure observed at Earth. They considered the implication of the heliolatitude independence of the magnetic flux density discovered by Ulysses (discussed below in more detail) for the currents in the corona, and concluded that only current sheets can exist rather than volume currents. The

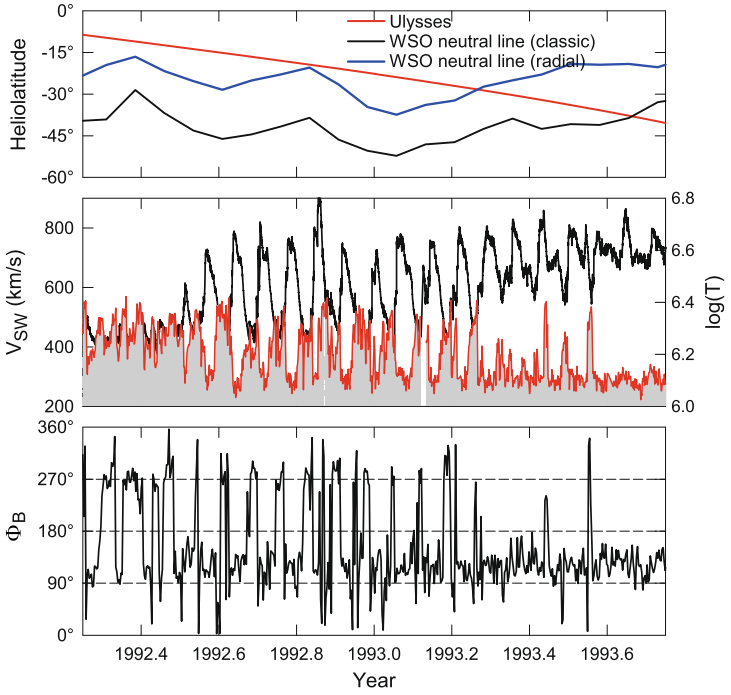

Fig. 5 *Upper panel*: the heliolatitude of the Ulysses spacecraft and the southern maximum extent of the source surface magnetic neutral line calculated using two different boundary conditions; *middle panel*: solar wind speed (*black line*, *left-hand axis*) and the coronal temperature of the solar wind source region (*red line*, *right-hand axis*) corresponding to the Ulysses observations; *lower panel*: the azimuth angle of the heliospheric magnetic field indicating the persistence of the sector structure to mid 1993

current sheet model as well as the PFSS model were found to provide a good match to the observations of both the polarity and the magnitude of the radial component of the magnetic field, provided that the appropriate corrections were made to the measured photospheric magnetic field.

The comparison between the solar source surface magnetic polarity and the polarity of the HMF was tested extensively during the Ulysses mission. Preliminary comparisons were made by Balogh et al. (1993) and Wang and Sheeley (1995), covering the in-ecliptic trajectory between the Earth and Jupiter and the first high latitude pass of Ulysses. Ulysses has been particularly suitable for testing the PFSS model because of its polar orbit and its coverage of the three-dimensional heliosphere through more than a complete solar activity cycle. In particular, as it first moved to high southern heliolatitudes, the spacecraft was immersed into fast solar wind from the then developing southern polar coronal hole and into a unipolar magnetic field, as the HCS was left equatorward of the spacecraft from ∼29° south (Smith et al. 1993).

In Fig. 5, the heliolatitude of Ulysses is compared to the maximum extent of the source surface magnetic neutral line calculated by two different techniques, together with the solar wind speed, the coronal temperature of region sampled by Ulysses and the magnetic field azimuth angle (i.e. the sector structure). The two PFSS calculations use different boundary conditions. The "classical" conditions set the source surface at 2.5 $R_{\odot}$, include a correction for the polar fields and assume a meridional component of the photospheric magnetic field.

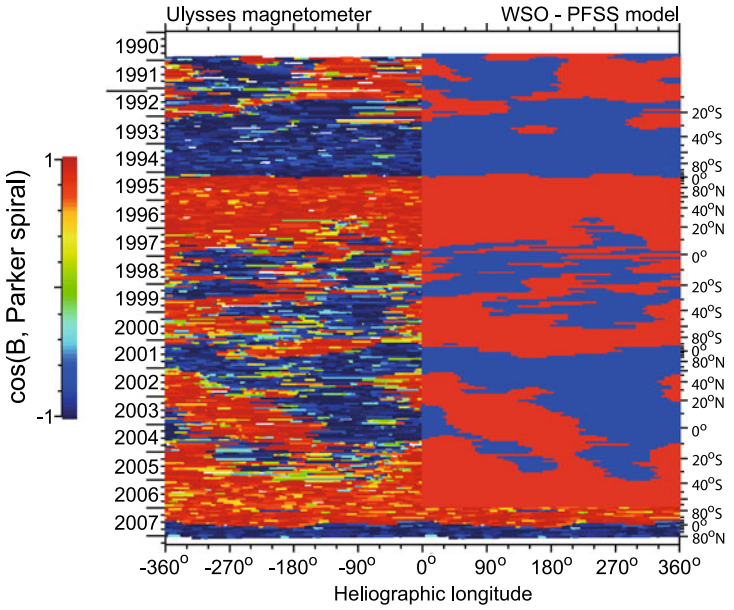

Fig. 6 Comparison of the magnetic polarities measured on Ulysses over its solar polar orbits from 1990 to the end of 2007 (*left half of the panel*) with the polarities expected at Ulysses by mapping back the location of Ulysses to the solar source surface, using the measured solar wind speed (*right half of the panel*). The match is in general very good, but degrades noticeably at high latitudes near solar maximum (the year 2000)

The "radial" conditions assume a source surface radius of either 2.5 $R_\odot$ or 3.25 $R_\odot$, require no polar field correction and assume a radial photospheric magnetic field. As Ulysses was moving to higher southern heliolatitudes in 1993, it entered the unipolar southern polar coronal hole field from mid-1993. A comparison of the disappearance of the sector structure, as well as the comparison of the coronal temperature and the solar wind speed with the crossing of the maximum extent of the source surface magnetic neutral line indicates that the PFSS model using the radial boundary condition was a better match for the Ulysses observations. However, Fig. 5 also shows that the neutral line (and the HCS) remained close to Ulysses at least until the heliolatitude reached that of the "classical" model. This comparison shows that the PFSS model is a very good guide the latitudinal extent of the HCS, and that the radial model (generally flatter, i.e. closer to the equator) performs better, but that clearly the proximity of the HCS to the observer makes the precise matching sensitive to the dynamic effects that can deform the HCS between its origin on the source surface and the observer.

Figure 6 shows the comparison between the magnetic polarities measured at Ulysses and the polarity expected from the PFSS model of the solar corona, taking the polarity of the location which corresponds to "footpoint" of Ulysses, when the solar wind is mapped back to the source surface. The stackplot covers the whole Ulysses mission, from 1990 to 2008. The colour scale used for the Ulysses observations shows that there are deviations (when the average magnetic field vector is not parallel or antiparallel to the Parker angle calculated directly using the locally measured solar wind speed). This is not surprising, as the dynamics of interacting solar wind streams and coronal transients propagating to the heliosphere introduce significant deviations in the magnetic field direction. There were larger discrepancies during the epoch near solar maximum when the probe was at high heliolatitudes. (The comparison of the Ulysses observations with their solar sources was assessed by Wang and

Sheeley (2006).) As already mentioned, the PFSS model relies on the photospheric magnetic field measurements; these are considerably less accurate at heliolatitudes over 70°. In addition, the PFSS maps are prepared over complete Carrington Rotations, thus relying on the photospheric magnetic fields only slowly changing over a solar rotation. This is certainly not the case near solar maximum, independently of heliolatitude.

The shape of the HCS around solar minimum is well understood to be a tilted and/or warped surface corotating with the Sun with a characteristic peak-to-peak north-south extension of between 40° and 60° (Smith 2001; Riley et al. 2002). The extrapolation of this surface from the magnetic neutral line on the PFSS model surface into the heliosphere to larger heliocentric distances yields the well-known ballerina skirt. While the waviness of the HCS (due to the relatively small tilt of the solar dipole away from the solar rotation axis, and/or to the relatively small size of the solar magnetic quadrupole) remains small, it is relatively easy to assume its shape out to a few AU. However, two effects need to be taken into account. One of these is the cumulative effect of the solar wind dynamics even at low solar activity (as detailed in Sect. 3 below), as modelled by Pizzo (1994). It was found that by 5 AU folds appear in the HCS, simply due to the dynamic evolution of variations in solar wind speed resulting from the presence of slow and fast wind streams at a given heliolatitude as a function of longitude. By 10 AU, shocks associated with Corotating Interaction Regions and the progressing dynamical interaction between streams of different speed sharpen the folds in the HCS. The model by Pizzo (1994) has also found that by 20 AU, the HCS was embedded in uncorrelated speed, density and magnetic field features. This evolution has important consequences for the structures of the solar wind and magnetic field in the outer heliosphere as will be described further in Sect. 3.

The location of the HCS in the outer heliosphere has been estimated by comparing the incidence of polarities toward and away from the Sun at the two Voyager spacecraft. In 1994, during the declining phase of solar cycle 22 and corresponding approximately to the epoch during which Ulysses first observed the latitudinal extent of the HCS, Voyager 1 was at a distance ∼56 AU and at a heliolatitude ∼32°N, while Voyager 2 was at ∼43 AU and ∼12°S. Although the observations at Voyager 2 were limited due to instrumental problems, Burlaga and Ness (1996) found that the distribution of the azimuthal angle of the magnetic field was unipolar at Voyager 1 and bipolar at Voyager 2, with the direction of the magnetic field at Voyager 1 pointing away from the Sun, in accordance with the extrapolation of the PFSS model. At Voyager 2, the observed sector structure provided evidence for the HCS to extend to south of the location of the spacecraft, again in agreement with the PFSS model for the epoch. Unfortunately, Voyager 2 observations covered only about 50% of the year, therefore the comparison of the distributions away and towards the Sun could not provide conclusive information on the possible north-south asymmetry of the HCS that had been inferred from the heliolatitude dependence of cosmic ray intensities observed by Ulysses (Simpson et al. 1996) and was not found in the magnetic field observations (Erdõs and Balogh 1998, 2010).

Despite the simplifying assumptions in the PFSS model and its sensitivity to uncertainties in high latitude line-of-sight measurements of the magnetic field, it has proved to be a very useful tool in relating solar magnetic fields to the HMF at least to a few AU. The matching has been made both in three-dimensions, with the Ulysses observations, and at 1 AU in the ecliptic. It seems clear that the origin of the HMF in the open flux regions of the solar corona is well established, as is the sector structure and the relationship of the sector boundaries (HCS) to the magnetic neutral line calculated on the source surface.

3 The Heliospheric Magnetic Field Around Solar Minimum Activity

An important and unexpected discovery in the Ulysses magnetic field measurements was the apparent independence of the radial component of the magnetic field vector of heliolatitude (Smith and Balogh 1995; Forsyth et al. 1996). This result was first established when, in 1994–1995, Ulysses first scanned through the heliolatitude range from 80°S to 80°N, under low solar activity conditions, shortly before solar minimum. During that interval. Ulysses was immersed in high speed solar wind flows away from the equatorial region, from the southern and northern polar coronal holes. Figure 7 illustrates the heliospheric conditions. The low value of the charge state ratio of the O7+ to O6+ ions in the solar wind indicates low coronal temperatures (Geiss et al. 1995), corresponding to high speed solar wind from coronal holes.

The constant value of the normalised radial component of the magnetic field shows that the magnetic flux density is constant as a function of heliolatitude, with the implication that the magnetic pressure dominates in the open field regions which are the source of the (fast) solar wind. In Fig. 8, the magnetic flux densities in the two hemispheres observed during the solar minima in 1996 and 2008 are shown as a function of heliolatitude. The steady values are -3.5 and $+3.0$ nT AU^2 in the southern and northern hemispheres, respectively, in 1994–1997 and 2.4 and -2.0 nT AU^2, in the southern and northern hemispheres, in 2006–2008. The decrease of about a third from the earlier minimum is consistent with observations of the strength of the polar magnetic fields and their decrease in both hemispheres between the

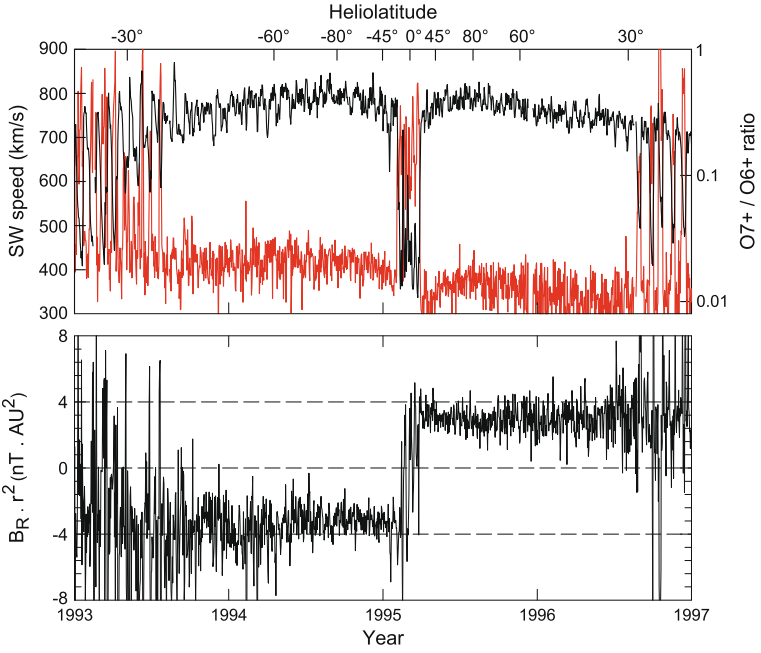

Fig. 7 The radial component of the HMF normalised to 1 AU over the solar polar orbit of Ulysses close to solar minimum shown in the *lower panel*; the solar wind speed (*black line*, *left-hand axis*) and the ion charge ratio O7 + /O6+ (*red line*, *right-hand axis*) are shown in the *upper panel*. As seen in the *lower panel*, the radial component of the magnetic field (a measure of the magnetic flux density) is independent of heliolatitude throughout the high speed coronal solar wind regime

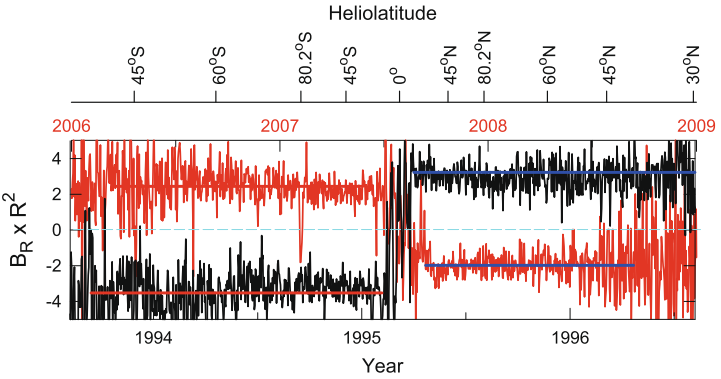

Fig. 8 The magnetic field density (the radial component of the magnetic field normalised to 1 AU) during successive solar minima as a function of heliolatitude in the two solar hemispheres. The 1994–1996 minimum is shown in black, the 2006–2009 minimum is shown in *red*. There was a decrease of about 30% between the minima in 1996 and 2008, successively

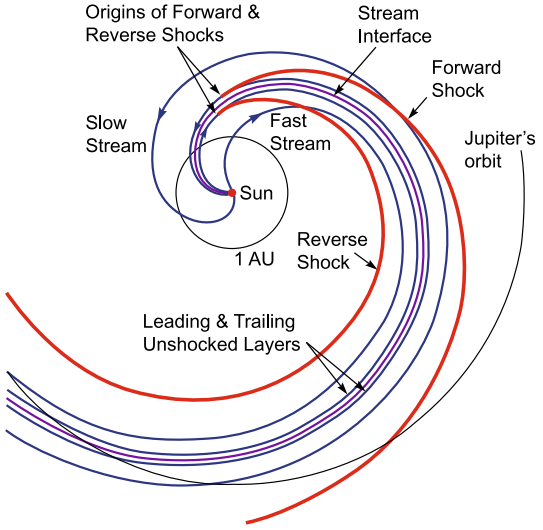

Fig. 9 Schematic representation of a simple Corotating Interaction Region

two solar minima (Wang et al. 2009) and the long term relationship between solar activity and solar magnetic fields (Zhou and Smith 2009).

Around solar minimum activity, the unipolar and uniformly distributed magnetic fields dominate the heliosphere, except in a relatively narrow band of 20° to 30° around the solar equator. However, in the equatorial region, fast and slow solar wind streams coexist at the same heliolatitudes. This results in the interaction between fast wind streams and preceding slow wind streams. The stream interaction regions (SIRs) form a persistent, corotating structure (to become Corotating Interaction Regions) when the sources of fast and slow solar wind are stable and recurrent in several successive solar rotations. The morphology of CIRs is illustrated in Fig. 9.

In the solar wind, the kinetic pressure of the following fast wind stream forms a region of compression on the two sides of the interface between the slow and fast streams. The compression generates a region of greater density, higher kinetic temperature and, at the

leading edge of the interaction region in the slow solar wind, a characteristic deflection of the flow (Gosling and Pizzo 1999). At the leading edge of the CIR, a pressure wave propagates into the slow wind while at the trailing edge, a pressure wave forms that propagates upstream into the fast solar wind. In general, from about 2 AU the pressure waves generally form shock waves, although some shock waves can form by the time the CIR reaches 1 AU. It appears that the steepening of the pressure waves to become shock waves occurs at distances from about 0.8 AU. At 1 AU, a long time-base study from 1995 to 2004 by Jian et al. (2006) found that about a third of CIRs observed at 1 AU had either a forward or a reverse shock wave associated with it. There seemed to be more forward shocks than reverse shocks. In many cases the shocks were quite weak. A later in-depth study of three CIR intervals, using multiple spacecraft data by Jian et al. (2009) found that the shocks formed at 1 AU may in fact be marginal and that the reversion of shock waves to pressure waves still occurs. However, at greater distances, as foreseen by modelling (Hundhausen 1973), shock pairs form regularly out to 5 AU and beyond (Smith and Wolfe 1976; Gosling et al. 1976; González-Esparza and Smith 1996) although the majority of shock waves generally remain weak (Balogh et al. 1995).

A well-documented series of CIRs was observed by Ulysses in 1992–1993 (Bame et al. 1993; Smith et al. 1993) has been shown in Fig. 5. Other series at 1 AU had been analysed earlier by Gosling et al. (1978) and Jian et al. (2006) and also between 1 and 10 AU by González-Esparza and Smith (1996). The dynamics of stream evolution beyond 1 AU is increasingly dominated by the colliding of successive CIRs, the interaction between the reverse shock of the preceding CIR with the forward shock of the following CIR. These dynamic interaction processes can only be modelled and qualitatively verified by observations at different heliocentric distances. Generally speaking, the method of evaluating the effect of merging shock waves starts with time series observations of the solar wind at 1 AU and uses quantitative non-linear modelling of the dynamics at larger heliocentric distances (Whang and Burlaga 1985; Whang 1991). The matching, or predictive ability of such models has been tested over an extensive set of heliospheric data by Zieger and Hansen (2008). Using solar wind observations at 1 AU, they predicted the solar wind speed and density, the magnetic field magnitude and the times of shocks at various spacecraft at distances >1 AU. The predictions were then compared to actual observations by the Pioneer and Voyager spacecraft. They have found that when the solar wind streams formed a recurrent series at 1 AU (such as during the late declining phase of the solar cycle) the predictions had a high correlation with the observations. During more active periods, when the solar wind speed was more variable from one solar rotation to the next, the predictive ability of the non-linear solar wind propagation model was less successful.

The complexity of the interactions at larger heliocentric distances can be discerned already at 1 AU during intervals of higher solar activity, but away from activity maxima. While the Sun is still relatively active, but already presents coronal holes of sufficient size and stability for fast solar wind streams to form, the dynamics in interplanetary space will be between successive transients (generally small Coronal Mass Ejections) and slow, variable speed streams, as well as the occasional high speed stream. One such 12-day interval was analysed by Burlaga et al. (2003a), illustrated in Fig. 10. They have found that due to the merging of interacting streams and structures, it was not possible to reconstruct the evolution of the different streams, based on the conditions in the corona. The analysis of the solar wind and magnetic field parameters showed that a likely scenario for the interval designated as (1) in Fig. 10 involved the interaction of two episodes of coronal ejecta with a magnetic cloud (MC, discussed in more detail below, in Sect. 4) and two shock waves to form a Merged Interaction Region (MIR) at 1 AU. MIRs in general arise from the dynamic

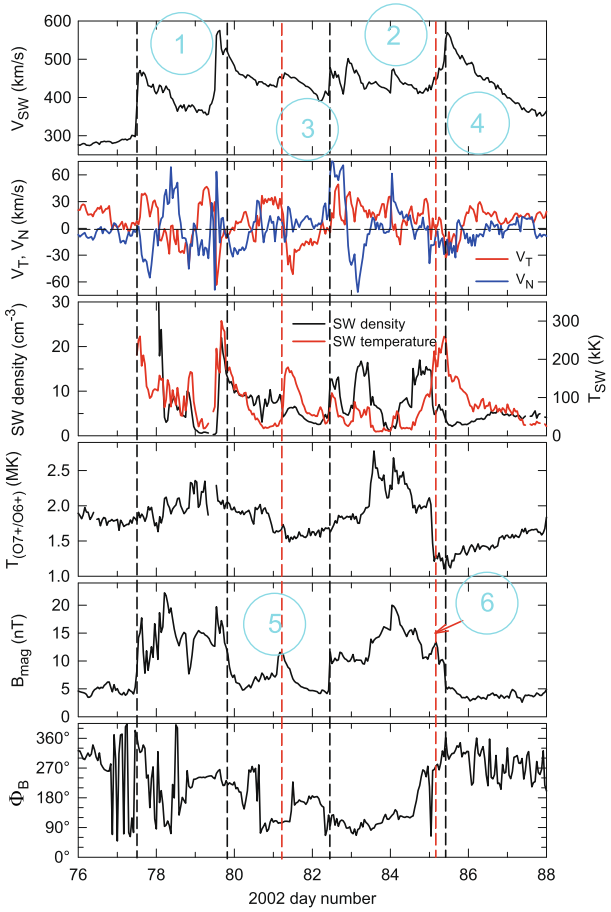

Fig. 10 A complex interval at 1 AU observed by ACE. The *top three panels* show the solar wind speed, the transverse components of the velocity, the density and the kinetic temperature; the *fourth panel* shows the coronal temperature derived from the oxygen ion charge ratio (the freezing in temperature); the *lowest two panels* show the strength and the azimuthal angle of the magnetic field. The solar origin of the solar wind and the dynamic effects in this interval were analysed by Burlaga et al. (2003a)

coalescing of individually formed solar wind features in which the dynamic interaction of unequal velocity plasma (from slow and fast streams, or from propagating solar wind transients) compress the solar wind to form regions of higher density and higher magnetic field leading to higher total plasma pressure (Burlaga et al. 1983). Interval (2) in Fig. 10 was also considered to result from the interaction of a corotating stream, two coronal ejecta, a MC and at least two shock waves. Intervals (3) and (4) indicate two corotating streams, while intervals (5) and (6) have been identified as Corotating Interaction Regions. It is noted that the successive interactions result in complex deflections as shown by the transverse components of the solar wind velocity vector and a general lack of correlation among the parameters such as the magnitude of the magnetic field, the solar wind density and kinetic temperature. The coronal temperature calculated from the charge state ratio of oxygen ions indicates that in fact much of the 12-day interval was dominated by slow solar wind streams (of different speeds) at temperatures greater than 1.5 MK, together with shorter intervals, associated with the coronal ejecta, at temperatures in excess of 2 MK. The only truly high speed solar wind stream was observed from day 85, when the coronal temperature dropped significantly below 1.5 MK. This interval provides evidence for the complex merging that occurs between solar wind streams; when the Sun is less active and transients do not occur with the same frequency as in the interval used as an example by Burlaga et al. (2003b),

the decorrelation of the solar wind and magnetic field parameters occurs at larger distances, although the cause, i.e. the dynamical merging processes between streams and interaction regions is effectively the same.

In general terms, the propagation, interaction and merging process between streams is quite complex, but the dominant effect, the merging of interaction regions appears to start at distances less than 10 AU and proceed to beyond 20 AU (Smith 1989; Burlaga et al. 1990; Gazis 2000). In Fig. 11, the magnetic field magnitude measured during the year 1984 (during the declining phase of solar cycle 21) is shown at four different heliocentric distances, measured by ISEE-3 at 1 AU, by Voyager 2 between 13 AU and 15 AU, by Pioneer 11 between 15 AU and 17.5 AU and by Voyager 1 between 18.5 AU and 21.5 AU. The merging of the large number of interaction regions characterising the solar wind conditions at 1 AU into large-scale, magnetically highly compressed regions appears to occur at distances less than ∼12 AU. The merged regions appear quasi-periodic, at the rate of approximately one such region per solar rotation. It was found by Burlaga et al. (1990) that for a well-observed series of CIRs at the rate of two per solar rotation at 1 AU some merging occurred (but leaving a recognizable two-stream structure) by ∼4.5 AU at Pioneer 11 but that the dominant periodicity of the interaction regions was one per solar rotation at 5.5 to 6 AU at Pioneer 10. The cause of the coalescing of the interaction regions was not simply merging by sweeping up of a slower interaction region by a following faster one, but by the spreading of all the higher pressure regions with heliocentric distance. Although further evolution will occur at larger distances, between ∼12 AU and ∼25 AU, the main effect of the propagation to these larger heliocentric distances appears to be the decrease in the magnetic field amplitude through the stretching of the field lines as the solar wind expands.

In the outer heliosphere, extended observations of the HMF and the solar wind plasma have only been made by the two Voyager spacecraft (see Fig. 1). A comparison between observations made in the two years, 1983 and 1994, that corresponded to the declining phase of two consecutive solar cycles showed that the quasi-regular and relatively well understood evolution to ∼14 AU could not be extrapolated to the larger distance ∼43 AU in the later interval (Burlaga et al. 1997). As illustrated in Fig. 11, the magnetic field magnitude shows a regime of MIRs, with a quasi-periodicity at the rate of the solar rotation out to ∼20 AU. However, Burlaga et al. (1997) found that the magnetic field magnitude became aperiodic and irregular by ∼43 AU; this behaviour contrasts with that of the solar wind speed which appeared aperiodic at 14 AU but became quasi-periodic at 43 AU.

In modelling the dynamics of the solar wind to ∼20 AU, Pizzo (1994) found that that the compressive structures (corresponding to high magnetic field intensities and solar wind densities) are concentrated around the developing folds in the HCS. These were found to form at the rate of one in each solar rotation. This evolution of structures corresponds to the observed characteristic periodicity of the compressive parameters at these middle distances illustrated in Fig. 11 for the magnetic field strength. The evolution of recurrent streams from initial conditions based on Voyager observations at ∼14 AU to distances potentially out to the Termination Shock was modelled by Whang and Burlaga (1988). The emphasis in the model was on the interaction of the forward and reverse shocks bounding the Corotating Interaction Regions as they propagated to greater heliocentric distances. The interaction of the shocks led to an increase in the temperature and pressure of the plasma and in the formation (and reformation) of compressive regions.

Observations through 1994, corresponding to heliocentric distances between 42 AU and 44.5 AU at Voyager 2 are shown in Fig. 12. This epoch corresponds to the declining activity phase of solar cycle 22, during which the extended sequence of CIRs observed at distances less than 5 AU had already been described above. Coronal conditions were clearly appropriate to introduce fast and slow solar wind streams at the heliolatitude of Voyager 2 that varied

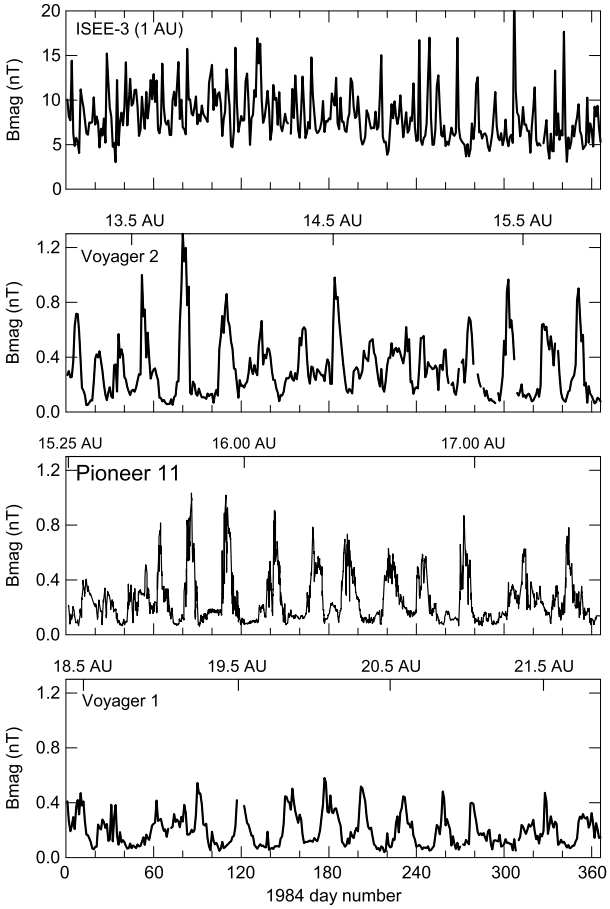

Fig. 11 The magnetic field magnitude measured through 1984 at four different heliocentric distances between 1 AU and 21 AU. The stream interaction regions at 1 AU (represented by their corresponding magnetic compression regions) merge into consolidated compression regions by the time the solar wind propagates to ∼13 AU. Although more dynamic interactions between streams may occur between 13 and 20 AU, the general pattern of about one large-scale compression region per solar rotation remains qualitatively unchanged

from 10.8°S to 13.1°S in 1994, equatorward of the maximum heliolatitude (∼30°S) of the Heliospheric Current Sheet determined by Ulysses. The sudden, shock-like increases in the solar wind speed at Voyager 2 recurred at the rate of the solar rotation—14 such increases are indicated in Fig. 12. (The nature of the abrupt increases is difficult to determine because of the statistics of the data; however, most of them seem to be accompanied by significant heating plasma.) It is very tempting to associate these increases with stream interactions, although was as shown above, at smaller distances (between 10 and 20 AU) the solar wind speed appears to be largely uncorrelated with the solar rotation, while the magnetic field magnitude is strongly correlated. It is unclear whether the Voyager 2 observations represent a restructuring of the more chaotic state of the solar wind speed or rather a series of corotating merged events that have travelled to greater distances in less disturbed conditions than the merged streams observed at ∼15 to 20 AU. As can be seen in the magnetic field magnitude and in the solar wind density, these parameters which are particularly sensitive to cumulative compressions are not correlated with the solar wind speed. However, the kinetic indicators, speed and kinetic temperature, appear to be strongly correlated.

The sector structure was found to remain recognisable out to the largest distances explored by the Voyager spacecraft to the Termination Shock. These large distances were covered mostly during the rising, maximum and early declining phases of solar cycle 23,

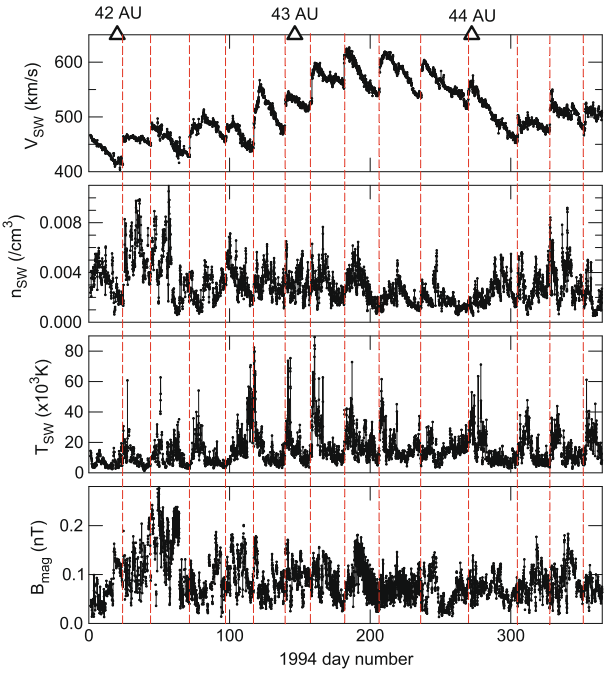

Fig. 12 Solar wind plasma speed, density and temperature (*upper three panels*) and magnetic field strength (*lower panel*) measured at Voyager 2 in 1994. The heliocentric distance of the measurements is indicated along the top

from 1998 to 2005. It was found by Burlaga et al. (2003b) that the sector polarities at the two Voyager spacecraft, that were located in opposite solar hemispheres were consistent both with the expected solar polarities and with the increasing heliolatitude reach of the Heliospheric Current Sheet. However, no compressive (high magnetic field strength) features could be associated with the sectors, at least partly because of the very small magnitude of the magnetic field (generally below 0.1 nT).

A comparison of the magnitude of the magnetic field measured over the ten-year interval from 1995 to 2005 at 1 AU and at Voyager 1 is shown in Fig. 13. Voyager 1 travelled from 58 AU to 94 AU during the interval. Remarkably, the magnetic field magnitude remains approximately in the range 0.025 to 0.075 nT over this heliocentric distance range, although there are very large variations from 1999 due to the propagation of large transients associated with solar events around solar maximum activity. Clearly, the magnetic field in the outer heliosphere remains subject to propagating dynamic structures out to the Termination Shock (that Voyager 1 crossed in December 2004). A particular feature of the magnetic field is that around solar minimum (from 1995 to late 1998) it showed a steady mean value but a clear variability of $\Delta B/B \sim 1$. During the later epoch, around solar maximum, the mean was variable and there were also very large transient excursions, although the variability was, similarly, about $\Delta B/B \sim 1$.

The degree of correlation among various parameters of the solar wind and the predictability from modelling the evolution of the dynamic structures have been limited by the observations limited to the two Voyager spacecraft. (Even these are limited further by instrumental problems affecting the solar wind plasma and magnetic field measurements on the two spacecraft.) An implicit limitation is the effect of the changing solar activity; as indicated in Fig. 13, the heliocentric distance changes by several tens of AU over the solar cycle. As far as low solar activity conditions are concerned, the interacting and merging streams observed at distances less than ∼20 AU become uncorrelated and the end result at larger distances,

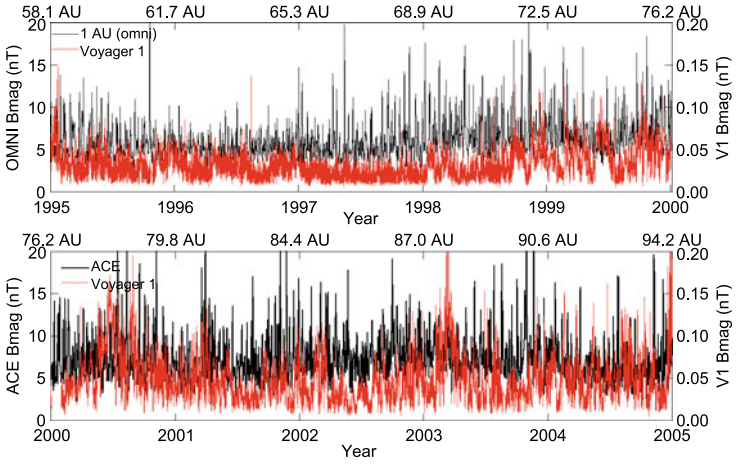

Fig. 13 Comparison of the magnetic field magnitude measured at 1 AU and Voyager 1. In the *upper panel*, the 1 AU measurements are taken from the OMNI database (IMP-8, ACE and WIND), while in the *lower panel*, the 1 AU data are ACE. Note that there is a factor 100 between the scales at 1 AU and Voyager 1. The heliocentric distance of Voyager 1 is shown along the top axes of the panels

as illustrated in Fig. 12 above, is an ordering that cannot be simply propagated from 1 AU by MHD models, according to the observations. Although it is possible that the evolution could be modelled (Wang and Richardson 2005) given the appropriate initial conditions and observations at a range of heliocentric distances, the most likely view is that the random interactions between already compound streams leads to an effectively chaotic structure in the outer heliosphere (Burlaga et al. 2003c).

4 The Heliospheric Magnetic Field Around Solar Maximum Activity

Contrary to the relatively simple and usually recurrent solar wind stream structure and its evolution (at least out to ∼20 AU) near solar minimum in the equatorial band of heliolatitudes, heliospheric condition around solar maximum activity are dominated by solar transients that occur at all heliolatitudes and introduce a very large degree of unpredictability in the observed solar wind and heliospheric magnetic field at all locations in the heliosphere. This applies also to the polar regions where the domination of the uniform high speed winds and the monopolar magnetic field near solar minimum is replaced by transients similar to those at lower latitudes.

Solar transients affecting the heliosphere as a result of chromospheric and coronal eruptions are the Coronal Mass Ejections that release up to about 10^{15} g of coronal material into the ambient solar wind. In the heliosphere, these event are often called Interplanetary Manifestations of Coronal Mass Ejections, or ICMEs. An extensive review of all aspects of CMEs and ICMEs can be found in Kunow et al. (2006). Within the ensemble of ICMEs, particular attention has been given to an important subset that retains the structure of the twisted magnetic loops in the corona which have then been ejected by the eruption.

The origin and formation of CMEs in the corona have been reviewed by Forbes (2000), Forbes et al. (2006), Hudson et al. (2006) and Vourlidas et al. (2010). For a general review of the signatures of ICMEs in the heliospheric magnetic field, see the review by Zurbuchen

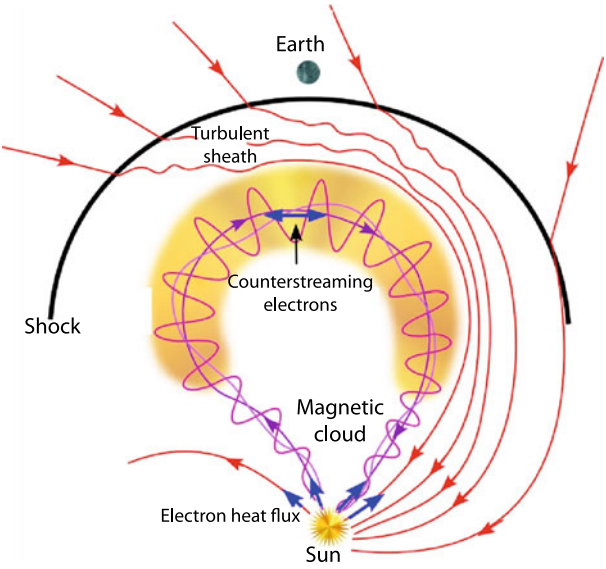

Fig. 14 A schematic representation of an ICME, indicating its major constituent parts. At the core of the ICME, there is in this figure a MC, showing the helical magnetic fields around the central axis of the magnetic flux rope. The counter-streaming electrons seen in the ICME are a sign that the flux rope is still connected to the corona at both ends. Preceding the MC that contains the coronal ejecta, more energetic CMEs often drive shock wave through the ambient solar wind. Behind the shock, and in front of the coronal ejecta, there is a sheath of shocked ambient solar wind. (After Zurbuchen and Richardson 2006)

and Richardson (2006) and references therein. There is a very large number of possible signatures, both in the solar wind plasma and in the magnetic field, but usually only a subset of these signatures is observed (Wimmer-Schweingruber et al. 2006 and references therein). The most often quoted structure (if statistically not the most frequent) of an ICME is shown schematically in Fig. 14 (after Zurbuchen and Richardson 2006). The magnetic structure of this CME is the magnetic cloud (MC) first described by Burlaga et al. (1981, 1982) and Klein and Burlaga (1982). However, only a third or less of the total number of ICMEs has been identified by a range of appropriate signatures show such a structure.

Magnetic clouds are flux ropes (e.g. Gosling 1990) that correspond to the evolved twisted magnetic loops in the corona that carry the ejected mass in the eruption. As illustrated in Fig. 14, the footpoints of the loops may be connected to the corona, hence the presence of counterstreaming suprathermal electrons (Zurbuchen and Richardson 2006), one of the key signatures of MCs. Although the schematic representation in Fig. 14 provides a first insight into the structure of CMEs, most ICMEs are more complex, for the reason that they consist of (presumably) complex loop structures in the corona that have been ejected into interplanetary space due to an explosive release of magnetic energy.

The rate of occurrence of CMEs observed remotely close to the Sun is a function of solar activity (Hundhausen 1993). There are significantly more energetic solar transients around solar maximum than solar minimum activity, although the largest solar eruptions (flares, CMEs) generally occur during the early declining phase of the cycle. A comprehensive survey of CMEs during solar cycle 23 derived from the observations of the LASCO coronagraph on the SOHO mission was carried out by Robbrecht et al. (2009) who compared the results of a CME list based on computer recognition and the visually established list from the observations. For the details of the comparison and its conclusion, see Robbrecht et al. (2009); Fig. 15(A) shows the overall occurrence rates of CMEs determined by the two method. Generally speaking, the automatic algorithm provides a list of CMEs which includes a range of smaller events, both in energy and in spatial and temporal extent, hence the larger rates determined by this method. However, it is clear, that there is a strong dependence on solar activity. It is also noted that the visually determined, larger CMEs indicate

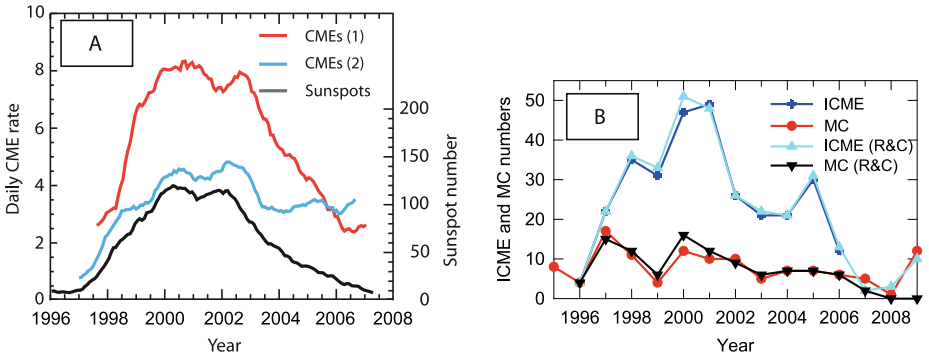

Fig. 15 Graph **A**: Occurrence rates of CMEs determined from SOHO LASCO observations during solar cycle 23 by two methods: CME(1) uses an automatic computer recognition technique, CME(2) is the visually determined list (CDAW). Both curves how that the rate of CMEs increases around solar maximum as indicated by the number of sunspots (*black line*). It is noteworthy that the decrease in CME occurrence rate during the declining phase of the unusually lengthened cycle is less apparent in the population of larger, visually identified CMEs. (After Robbrecht et al. 2009.) Graph **B**: The ICMEs and MCs observed by the WIND ACE and other near-Earth spacecraft through solar cycle 23. (Data from Wu and Lepping 2011, and Lepping et al. 2011; data—indicated as (R&C)—from Cane and Richardson 2003 and Richardson and Cane 2010)

more clearly the slower rate of decrease in solar activity, characteristic of cycle 23, while the more comprehensive survey using the automatic recognition algorithm indicates that there was a strong decline in the number of smaller CMEs in parallel with the decrease in sunspot numbers.

The numbers of ICMEs and MCs observed at 1 AU by the WIND spacecraft over solar cycle 23 are shown in Fig. 15(B) where the data were taken from Wu and Lepping (2011), Lepping et al. (2011) and Richardson and Cane (2010). The determination of the exact proportion of MCs is difficult, in part due to the variety of observations and criteria and in part to the fact that observations are in majority by a single spacecraft which may provide a view of only the flanks of an ICME. Wu and Lepping (2011) have identified 103 MCs and a total number of 307 ICMEs at 1 AU, covering the years from 1996 to 2006. For a longer interval, from 1996 to 2009, Richardson and Cane (2010) have identified, using somewhat different selection criteria, 322 ICMEs and 102 MCs. Thus the proportions of MCs are 33% in the former study and ∼32% in the latter study.

There is of course a significant difference between numbers of CMEs observed on the Sun and the numbers of ICMEs (including MCs) that are observed at a given point, i.e. close to the Earth, at 1 AU, in interplanetary space. *In situ* observations are significantly limited for observing these travelling transient events to those that include the observing spacecraft in its volume. This simple geometrical argument explains in general the difference between the detection of CMEs on the Sun and in situ in the form of ICMEs at 1 AU. However, there are solar-cycle dependent differences between the rates. These were investigated by Riley et al. (2006b) who found evidence that there was a divergence between the numbers of CMEs and ICMEs during the ascending phase of solar activity from 1998 when the mid-heliolatitude active regions on the Sun appeared and that there was an increase in the number of CMEs that may not have been detected in situ in the ecliptic. The solar latitude dependence of occurrence of CMEs as a function of solar activity is thus superimposed on the simple geometric argument and implies that the angular extent of CMEs (itself a function of heliolatitude, and changing with solar activity) also affects their interplanetary counterparts. In this way, the phase of the solar cycle has a marked affect on which transient events reach

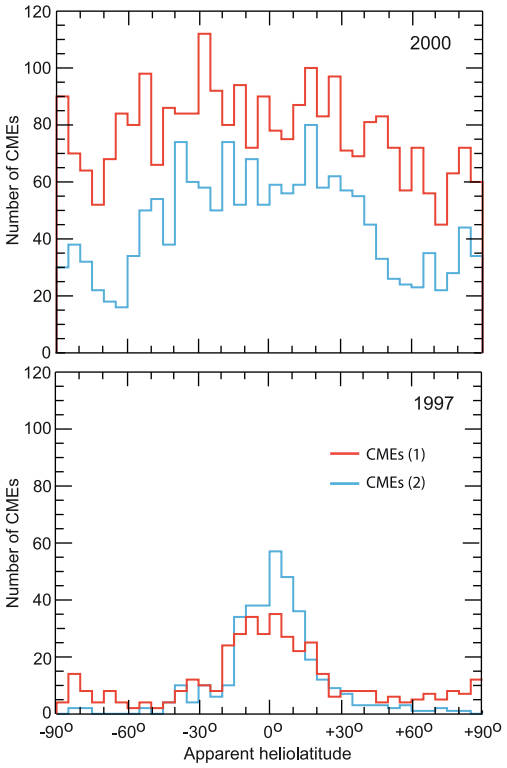

Fig. 16 The variation in the number of CMEs as a function of apparent heliolatitude between solar minimum and solar maximum. CMEs are much less frequent near solar minimum and are restricted to the equatorial streamer belt at solar minimum while the much larger number of CMEs near solar maximum is distributed more uniformly at all heliolatitudes. For the labelling of the curves, see Fig. 15, graph A. (After Robbrecht et al. 2009)

the Earth. This effect also contributes greatly to the difficulties of determining the solar origin of any but the most energetic solar transients that reach the Earth. However, because of the implications of ICMEs for the Earth's space environment (space weather), the study of the subset of CMEs reaching the Earth is important in itself, but it also provides a representative sample of transient events affecting the whole volume of the heliosphere, if the special solar cycle associated selectivity effect is taken into account. The general argument is also important for the solar cycle modulation of cosmic rays: the way in which ICMEs and MCs affect the 3D structure of the heliospheric magnetic field is dependent on solar activity levels and the frequency and heliolatitude distribution of CMEs.

Another characteristic of the solar cycle dependence of CMEs is their distribution in heliolatitude. As shown in graph A, Fig. 16 (adapted from Robbrecht et al. 2009), CMEs close to solar minimum are confined to an equatorial band around 45° to 60° in north-south extent, characteristic of the distribution of coronal streamers. However, close to solar maximum, CMEs are distributed over the whole range of latitudes from the south to the north polar regions. Although restricted in solar cycle coverage, the study by Hundhausen (1993) had already indicated clearly the much broader distribution of CMEs in heliolatitude near solar maximum in 1980 and 1989 than nearer solar minimum in 1986. An interesting feature of the CME occurrence rates shown in Fig. 16 is the much larger difference between rates detected by the computer-based recognition algorithm (curve CMEs 1) around solar maximum and the rates derived visually. This means that there is a preponderance of smaller transients near solar maximum, and by comparing this with Fig. 16, these smaller transients are more frequent at all heliolatitudes. This has implications for the distribution of transient

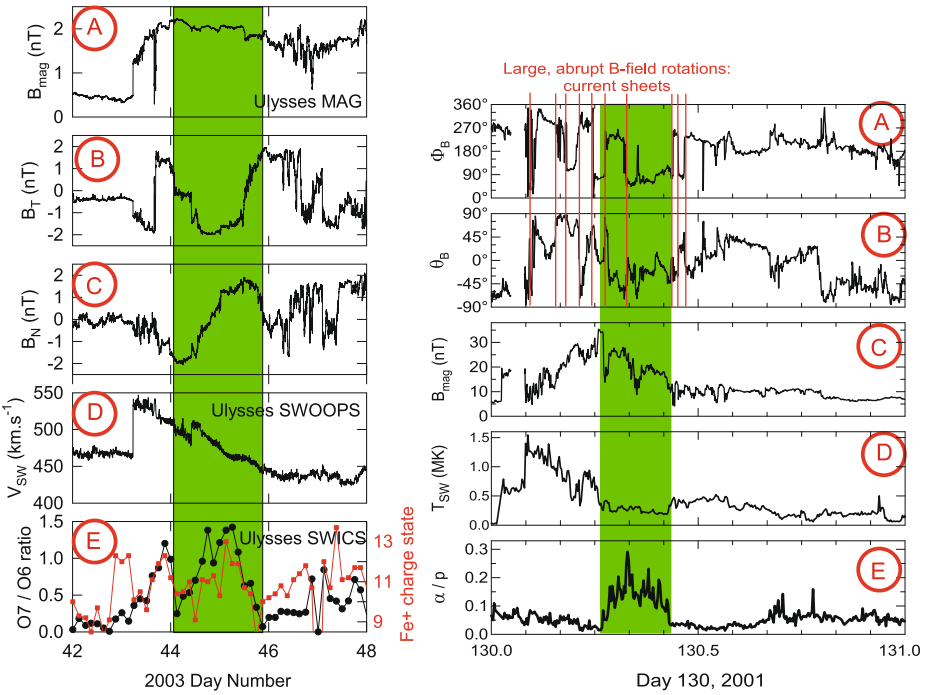

Fig. 17 Two examples of Interplanetary Coronal Mass Ejections. *On the left*, a "classic" MC is shown with its characteristic leading shock wave, large magnetic field (panel **A**), large scale magnetic field rotation (panels **B** and **C**), large jump in solar wind speed followed by a steady decrease (panel **D**), and high coronal temperature signatures (panel **E**). *On the right*, a short duration, but complex CME, with a reduced solar wind temperature (panel **D**) and an enhanced alpha proton ratio (panel **E**), increase in the magnetic field strength (panel **C**), and complex, abruptly varying magnetic field direction (panels **A** and **B**), indicative of the presence of current sheets separating plasmas of different origins from the corona. In both panels, the *green shading* represents the characteristic CME material

heliospheric magnetic structures at solar maximum: the smaller, but more frequent transients lead to the formation of rapidly evolving MIRs at high heliolatitudes.

In Fig. 17, two ICME examples are given. In the panel on the left, the enhanced magnetic field strength (panel A) and the large-scale rotation of the magnetic field, represented by its transverse components (panels B and C) indicate that the dominant part of the event is a MC. Both the magnetic field and the solar wind speed indicate the presence of a leading shock wave. The solar wind composition observations (panel E) however indicate some complexity in the event. The ratio of the charge states of oxygen ions in the solar wind O7 + /O6+ is a measure of the coronal temperature of the solar wind plasma (the freezing-in temperature), see, e.g., von Steiger and Zurbuchen (2003) who used a value of this ratio greater than 1 (corresponding to a freezing in temperature in excess of 2.15 MK) as a threshold for identifying possible ICMEs. The average charge state of iron ions, also plotted in this panel E, has been determined to be in excess of 12 for ICMEs (Lepri et al. 2001). Both these coronal temperature indicators agree about the presence of an ICME in the form of a MC corresponding to the rotation in the magnetic field.

The event shown in Fig. 17 (right panels) presents a different magnetic structure. Here the solar wind alpha/proton ratio and the solar wind temperature are used to identify the ICME. However, both preceding and following the region of high alpha/proton ratio and

reduced solar wind temperature, there are magnetic field rotations that are abrupt, indicating the presence of multiple current sheets associated with the ICME. This is an example of an event that is not a simple MC, although it illustrates one important aspect of many ICMEs: their magnetic complexity. Although the event is of short duration compared to the typical duration (>1 day) of a MC, this is due to the superposition of several different magnetic field regions, almost certainly originating as a multiple loop system forming the CME in the corona. This short-duration event is in fact different, because of its magnetic structure, from short duration flux ropes discussed below.

Modelling CMEs and ICMEs has provided an insight into the large scale, 3D extent of their structure and dynamics (Forbes et al. 2006 and references therein). The initiation, coronal trajectory and interplanetary evolution of CMEs have been modelled by using 2D and 3D MHD techniques (e.g. Cargill and Schmidt 2002; Odstrcil et al. 2003; Riley et al. 2004, 2006a and references therein). The many questions concerning their initiation and propagation (Schwenn 2000) have not all been answered as yet, but the increasing sophistication of the technique has led to a better understanding of their dynamics and a more realistic shape than the simple circular cross section flux rope (Riley and Crooker 2004).

Magnetic clouds have been, nevertheless, traditionally modelled as force free flux ropes (Burlaga 1988). The technique has been described in detail (e.g. by Lepping et al. 1990) and used extensively to determine the structure of MCs . In a force free flux rope, the current density is proportional to the magnetic field vector, with a constant of proportionality denoted by α. When α is taken to be invariant throughout the flux rope, the equation to be solved for the magnetic field is $\nabla^2 B = \alpha B$ that yields an axially symmetric solution, with magnetic fields in the form of helices around the axis of the flux rope. (The simplified sketch of an ICME shown above in Fig. 14 contains a MC.) The helical magnetic fields of the flux rope in fact form a three dimensional structure, rather than the idealized cylindrically symmetric form as modelled by the force free approximation. The helix is progressively tightened the further it is away from the axis of the flux rope. A spacecraft, observing as a MC travels past it, records a characteristic large scale rotation in the magnetic field. At the same time, the strength of the magnetic field increases, with a maximum at the closest approach of the spacecraft to the axis of the flux rope. The "classic" MC shown on the left in Fig. 17 is an example when these two magnetic characteristics are clearly seen.

In general, modelling MC associated with ICMEs using this flux rope model has been quite successful. In Figs. 18a and 18b, two examples are shown. In Fig. 18a, the MC is in fact not a simple flux rope, but it consists of two flux ropes, as shown by the fit (Rees and Forsyth 2004). In some cases, ICMEs and the MCs they contain result from multiple coronal loops, some interacting and others propagating in tandem at the local solar wind speed (Wang et al. 2002b, 2005). Even when the MC is a single flux rope, its shape is certainly subject to possible deformations as it evolves dynamically while propagating in the solar wind. A relatively simple deformation, yielding a relatively flat magnetic field magnitude profile, results in an oblate shape which can yield a better fit to the observations, as shown in Fig. 18b, from Vandas et al. (2006). An iterative fitting procedure that also relaxes the circular symmetry of the simple force free flux rope model has been developed by Démoulin and Dasso (2009) who have found that a more realistic oblate model provides more information on the MC related to overall flux values and magnetic helicity.

Modelling ICMEs and MCs remains an active area of research, because of the importance of solar transients on the Earth's space environment. New techniques, such as the 3D reconstruction of spatial structures using the Grad-Shafranov equations (Sonnerup et al. 2006) have been applied to MCs (Möstl et al. 2009) that provide a three dimensional view

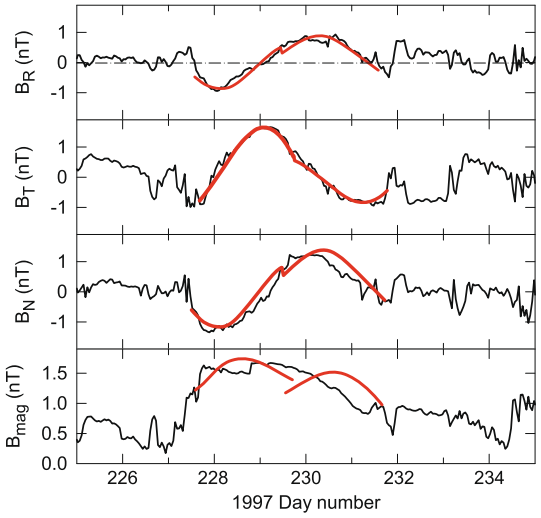

Fig. 18a An ICME that consisted of a double flux rope observed by Ulysses at 5.2 AU near the ecliptic. The complexity of a double flux rope can be treated, but possibly not uniquely, by matching two consecutive, but not colliding flux ropes, using the techniques developed for single flux ropes. The *red curves* represent the fits to the components and the magnitude of the magnetic field. (After Rees and Forsyth 2004)

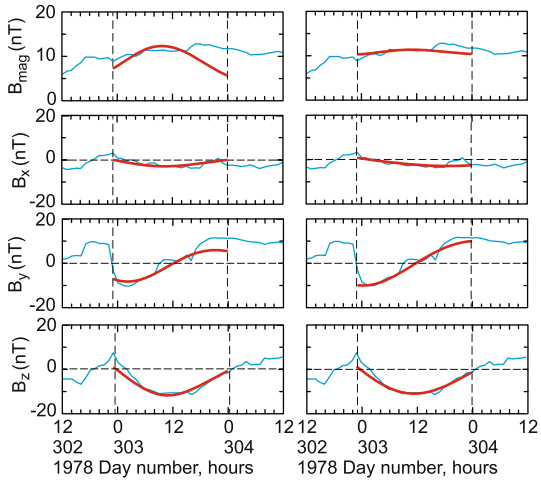

Fig. 18b Comparison of two flux rope models applied to the same ICME by Vandas et al. (2006). *On the left*, the flux rope model applied is that of a circular cylinder, while *on the right* an oblate cylinder model is used. It seems clear, that while some MCs can be represented by the simple circular flux rope model, to many others a more deformed model is more appropriate (Riley and Crooker 2004). In this case, the MC has a relatively flat profile of the magnitude of the magnetic field, indicating an oblate object

and a much more detailed reconstruction of the internal parameters. Although these reconstructions provide much information on the possible or probable structure of the ICMEs and their embedded MCs, observational confirmation is in general difficult to obtain. An investigation of estimating the magnetic field line length in MCs using the measured travel time of energetic solar electrons (Kahler et al. 2011) has concluded that the apparent path length is mostly shorter than expected by the twists implied in magnetic flux ropes. This result confirms that while flux ropes provide the right interpretation for the observed MCs, the flux rope models need to include more complexity to represent the variety of dynamic structures that will be present in ICMEs.

Short duration magnetic flux ropes, defined as lasting only hours, appear to constitute a special class of magnetic structures in the solar wind. First detected by Ulysses at 5 AU in the ecliptic, in a background of slow solar wind, it was considered to be on non-coronal origin, but rather a signature of interplanetary magnetic reconnection (Moldwin et al. 1995). Their frequency is greater than that of classical magnetic flux ropes. In the 10-year interval from

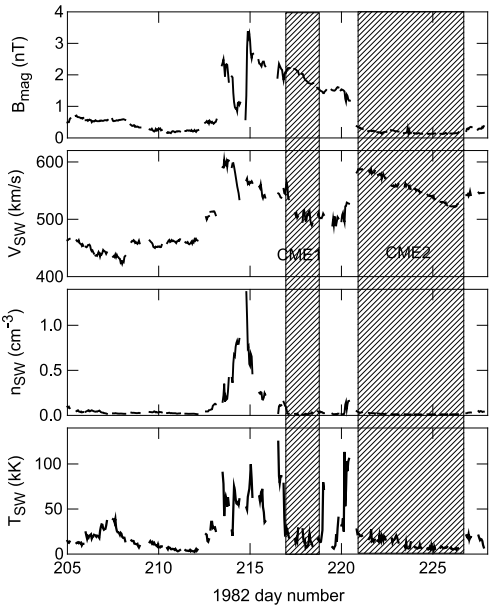

Fig. 19 Two transient events identified by Wang and Richardson (2004) as ICMEs at 10.5 AU, identified from their low proton temperature (*lowest panel*). As shown in this figure, the magnetic signature agrees with the first event (CME1) but the very low value of the magnetic field during the second interval (CME2) introduces a significant doubt about the nature of the transient. Ahead of the first event, there is a strong compression of the plasma, containing (probably) two forward shock waves

1995 to 2005 about 100 such MCs were identified by Cartwright and Moldwin (2008) and Feng et al. (2008). These small events occur almost exclusively in slow solar wind streams and travel at the speed of the ambient solar wind. Investigating their heliocentric evolution from the inner heliosphere (using Helios 1 and 2 observations), through 1 AU, to a few AU (Ulysses), Cartwright and Moldwin (2010) found that the flux ropes expanded significantly at distances less than 1 AU, but that there was no further apparent extension beyond 1 AU. They concluded that these short-duration flux ropes were not formed in the corona but that they originated close to the Sun in interplanetary space. However, their frequency, as a function off the solar cycle, matched that of classical flux ropes. They have been modelled in a similar way to ICME-associated flux ropes, their presence in the slow solar wind is both a relic of possible reconnection processes close to the Sun (in helmet streamers, possibly) and an added dynamic component in the evolution of the magnetic field.

Most of the observational and modelling data about ICMEs and MCs refer to the evolution and structure of these transients between the Sun and 1 AU. For heliospheric distances beyond ∼10 AU, the observations that identify solar transients are limited essentially to large-scale events associated with the largest solar eruptions. Smaller individual events (the majority of those seen at 1 AU) appear to become effectively unrecognisable through the dynamic evolution during their propagation to the outer heliosphere, similarly to the loss of ordering at larger distances of the well-ordered CIRs near solar minimum. The survey of ICMEs observed by Voyager 2 from 1 AU to 30 AU (from 1977 to 1989) by Wang and Richardson (2004) found a total of 147 transient events which were identified as ICMEs, based on abnormally low proton kinetic temperature, although, where possible, supporting information was used from other solar wind plasma and magnetic field measurements. As expected, it was found that recognising all ICMEs on the basis of this information is difficult, particularly from heliocentric distances greater than about 10 AU. Two such events, observed at 10.5 AU in 1982 (shortly after solar maximum) have been plotted in Fig. 19, illustrating the challenging nature of the drawing conclusions from the relatively sparse data available. The lack of information on solar wind plasma composition, in particular, leads

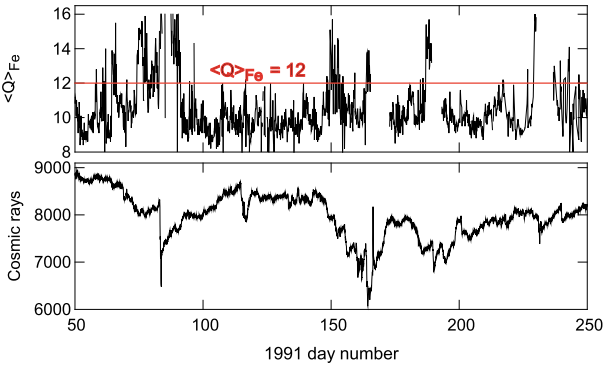

Fig. 20 In the *upper panel*, ICMEs observed by Ulysses in 1991 (as identified by the high average charge state of Fe ions, see Lepri et al. 2001); in the *lower panel*, the cosmic ray intensity measured by the McMurdo neutron monitor

to only relatively indirect signatures being available from the spacecraft that have reached large heliocentric distances.

A particularly active interval in the numbers and sizes of CMEs on the Sun occurred in 1991, shortly after solar maximum activity. A useful way to identify the ICME intervals is by the high proportion of the plasma in interplanetary space associated with CME material through the high level of ionization of iron ions as measured by the plasma composition instrument on Ulysses (Lepri et al. 2001; von Steiger and Richardson 2006). This is shown in Fig. 20. Also in Fig. 20, we show the measured ground level cosmic ray intensity in which the characteristic Forbush decreases represent the passage of the ICME that forms a barrier to their access to the inner heliosphere. This complex interval, with several groups of CMEs, ICMEs, as well as energetic solar particle events and Forbush decreases was described and analysed at 1 AU and in the outer heliosphere by McDonald et al. (1994). Figure 21 illustrates the magnetic field and plasma observations at three heliocentric distances, at the location of Ulysses (from 1.5 to 3 AU), Voyager 2 (at 34 to 36 AU) and at Voyager 1 (at 45 to 47 AU). It is not possible to show the same parameters for comparison at the three spacecraft, because of different and (in the case of Voyager 1) non-functional instrumentation. The magnetic field magnitude in all three cases shows the enhanced values associated with ICMEs; however, the events are better resolved at the distance of Ulysses, resulting in a number of shorter distinct increases, corresponding to individual ICMEs from the Sun. By the time any sequence of such ICMEs arrives at the distances of Voyager 2 and Voyager 1, the events have coalesced into large, long lasting enhancements of the magnetic field. At location of Voyager 2, starting around Day 150, 1991 (Fig. 21, middle panels), the enhancement in the magnetic field, the large increase in solar wind speed, density and temperature are the result of the evolving structures originating in the series of ICMEs observed by Ulysses around Days 80 to 90, 1991 (Fig. 21, left panels), caused by the series of solar flares and other intense solar transients in March 1991 (Belcher et al. 1993). The implied propagation speed is ∼650–700 km/s for this group of transients. The second MIR at Voyager 2, starting around Day 250, 1991, is likely to have resulted from the series of CMEs and ICMEs in June, 1991 (Burlaga and Ness 1994), corresponding to a transit speed of ∼550 km/s. At the more distant location of Voyager 1, only one large MIR was observed (Fig. 21, right panels). Only magnetic field data are available at this location. The components of the magnetic field show large-scale rotations, clearly indicating the deflection of the magnetic field by the dynamic processes that have led to the coalescing of the multiple ICMEs. It is likely that this large MIR was the evolving large-scale structure that coalesced from the ICMEs originating in March 1991, thus corresponding to a lesser transit speed of ∼430 km/s which is close to

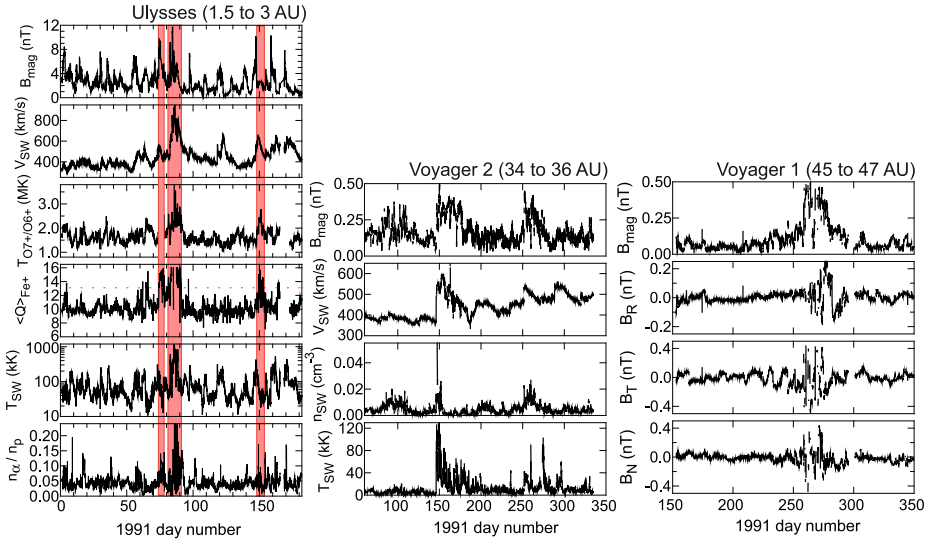

Fig. 21 Interplanetary magnetic field and solar wind observations in 1991 made at three different heliocentric distances, over comparable time intervals. *On the left*, observations by the Ulysses instruments included plasma charge composition measurements that provide unambiguous identification of hot coronal material. The *intervals shaded in red* correspond to intervals when the average ionic charge of iron was 13 or greater, identifying the ICME intervals, as shown by Lepri et al. (2001). The relationship among the observations is discussed in the text

the average transit time of the solar wind. At Voyager 1, the second series of ICMEs from June 1991 evolved into a more complex and longer lasting MIR in the first months of 1992, leading to a large and sustained drop in cosmic ray intensity as reported by McDonald et al. (1994).

One of the largest solar transient events of the last (23rd) solar cycle in the heliosphere was the so-called Bastille day event that occurred on 14 July 2000. The sequence of the near-Earth manifestations of the complex event was reviewed by Lepping et al. (2001). At the core of the event were two MCs, of which the second was the larger. Both were of relatively short duration, the first of 8 hours, the second, very intense one, 14 hours. There were other magnetic and compositional signatures of ejecta in the events arising from the solar transient, including multiple current sheet crossings and both density and magnetic field enhancements. Taking the solar wind and magnetic field profile of the events at 1 AU, Whang et al. (2001) used a MHD model to construct the evolution of the composite event arising from the interaction of the components: shocks, MCs and other signatures of coronal ejecta from 1 AU.

They continued the modelling to 5.5 AU where a still-expanding very large MIR was identified, bounded by two shock waves, one forward and one reverse, still propagating and thus expanding the MIR. Thus the resulting structure at 5.5 AU was no longer recognisable as the sequence seen at 1 AU but has become a single, propagating large-pressure event that, because of the energy released in the original CME from the corona, created a global event for the heliosphere. The global nature of the event was emphasised by solar wind, magnetic field and energetic particle observations in the outer heliosphere at Voyager 1 (∼80 AU) and Voyager 2 (∼63 AU) by Burlaga et al. (2001), Wang et al. (2001) and McDonald et al. (2001).

In a review of magnetic field, solar wind and cosmic ray observations in the outer heliosphere, Burlaga et al. (2003d) examined in detail other large solar transients that reached the two distant spacecraft, Voyagers 1 and 2 and related MHD models that propagated the magnetic field solar wind observations at 1 AU to the location of the Voyager spacecraft. The model fits to the observations were able to match the arrival of a large MIR that formed from the transients observed at 1 AU, despite the difference between the heliographic longitudes between the observation points. This has led to the conclusion that MIRs, in particular what has been called Global MIRs (or GMIRs) due the largest events effectively form a quasi-spherical shell of enhanced magnetic field and solar wind density in the distant heliosphere that acts as a barrier to the access of cosmic ray access to the inner heliosphere. In addition, Burlaga et al. (2003d) have proposed an empirical, 4-parameter relationship between the intensity of cosmic rays and the magnitude of the magnetic field. The relationship provides a predictive match to the cosmic ray observations in its main features, however, in several details it fails quantitatively, as pointed out by Burlaga et al. (2003d), due to uncertainties in the magnetic field measurements and data gaps.

A case study of an ICME which was observed at Ulysses at 5.3 AU was tracked, using a one-dimensional MHD model, out to the location of the Voyager 2 spacecraft by Paularena et al. (2001). The complex profile of the ICME—treated as leading to a MIR—is shown in Fig. 22. An experimental problem that makes the identification of ICMEs at two distant locations very difficult is that only a very limited number signatures can be identified, for instrumental reasons, at both locations. Although in the case of Ulysses, the routine measurement of the ionic charge state distributions of carbon, oxygen and iron, in addition to the measurement of the relative alpha particle abundances provides in general a well defined signature of an ICME, the distant Voyager spacecraft are only equipped to a measurement of the alpha particle abundance which, if it is significantly higher (about 10% or more) than the average value is a sufficient, but not necessary condition for the presence of CME material in the ICME. The profiles of the observed parameters in the MIR, the solar wind density, speed and the magnitude of the magnetic field do not resemble profiles usually seen in the inner heliosphere, at 1 AU. In the event considered by Paularena et al. (2001), the alpha abundance signature was well recognised at both Ulysses and Voyager 2, and matched by the modelled evolution profile from 5.3 AU to 58 AU, as shown in Fig. 23. This, together with the decrease in the cosmic ray intensity shown in Fig. 22 provide the evidence for the interpretation of this event as a MIR arising from an evolution of ICMEs. (Note that the intermediate modelled profiles between the two locations have been omitted from this figure, although they are explicitly shown by Paularena et al. 2001.)

Variations in the interplanetary medium near solar maximum in the outer heliosphere show more puzzling features than simply the large transients that can be related to large solar events. The magnetic field and solar wind plasma at the location of Voyager 2 are shown in Fig. 24 (adapted from Wang and Richardson 2005) over a nearly two year interval following the last solar maximum. There appear to be no clearly recognisable MIRs during this long interval; however, the amplitude of the variations is large and appears to be quasi-periodic in solar wind speed and density, also in solar wind pressure and even in the magnitude of the magnetic field. In Fig. 24, the red line shows the modelled prediction of the plasma parameters propagated from 1 AU to the location of Voyager 2 using a MHD simulation. There appears to be a good agreement in a general sense for the pressure and the number density of the solar wind, but the fit is less good for the solar wind speed (Wang and Richardson 2005). The goodness of fit, even if moderate, is still interesting as it shows nearly in-phase large scale variations in the solar wind, although this is not the case at 1 AU. The magnetic field magnitude also varies (nearly in phase with the pressure variations). This

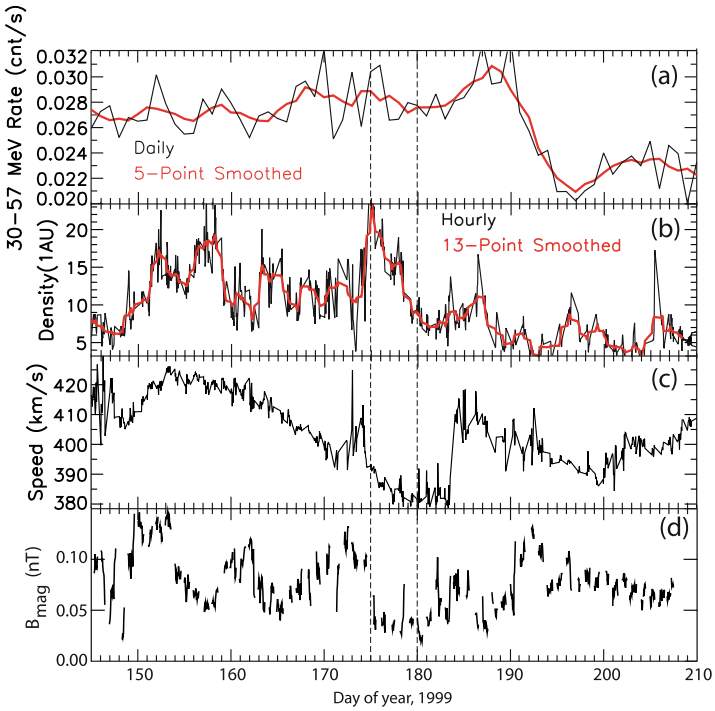

Fig. 22 Voyager 2 observations of a probable MIR at a heliocentric distance of 58 AU. (**a**) High energy particle intensity showing a long lasting drop (Forbush decrease) from ∼ day 190; (**b**) The solar wind density showing an enhancement from ∼ day 175, in coincidence with a very significant enhancement of the alpha to proton ratio (*interval between the vertical dashed lines*); (**c**) Solar wind velocity showing low speed wind during the enhanced alpha particle interval; (**d**) The intensity of the magnetic field showing a number of compression regions, but also a sudden drop in coincidence with the onset of the enhanced alpha particle interval. (Adapted from Paularena et al. 2001)

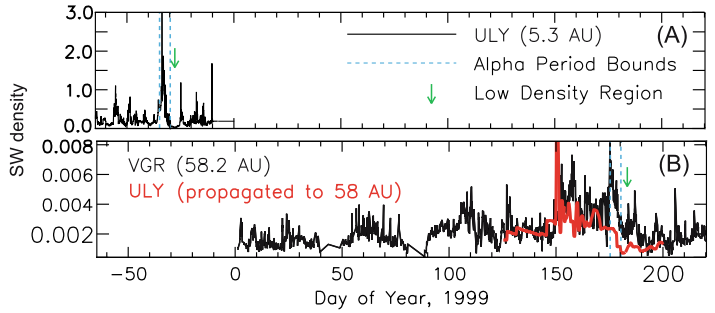

Fig. 23 Solar wind plasma density at (*upper panel*) Ulysses (5.3 AU) and at (*lower panel*) Voyager 2 (58 AU), showing the passage of an ICME at the two location. At Ulysses, there was a greatly enhanced alpha density as well as high values of coronal temperatures associated with the event, as measured by the charge state distribution of oxygen ions and the average electronic charge of iron ions. Using a one-dimensional MHD model for the propagation of the ICME, the timing and structure of the enhanced alpha region can be recovered at the location of Voyager 2. (Adapted from Paularena et al. 2001)

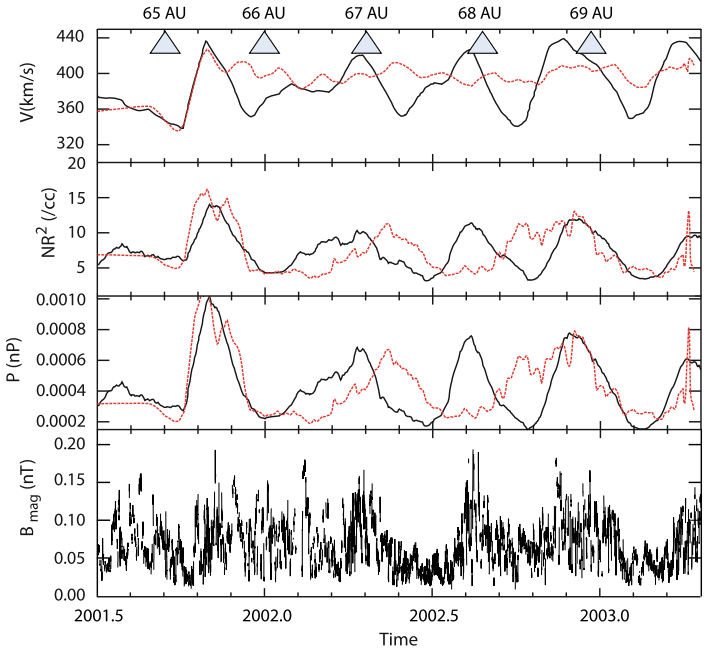

Fig. 24 Correlated, quasi-periodic variations of the solar wind speed, density and pressure, and of the magnitude of the magnetic field in the outer heliosphere near solar maximum observed by Voyager 2. The heliocentric distance of the observations is indicated along the uppermost horizontal axis. The *red dashed line* represents a MHD model that propagated the observations at 1 AU to the location of Voyager 2. It is unclear why variations typical of solar maximum conditions at 1 AU evolve to these very large scale structures. (Adapted from Wang and Richardson 2005)

ordering of the medium presents a different picture from that at distances ∼30 to 40 AU. Thus the evolution of even disturbed interplanetary conditions nearer the Sun results in a low-pass filtering of the variations but also an increase in the power in the variations at much larger scales.

A remarkable, and unique large shock wave was observed at the location of Voyager 2 at about 79 AU in 2006, relatively close to the Termination Shock (reached at 83.7 AU in August 2007). The event, shown in Fig. 25, has been studied by Richardson et al. (2006a). Unlike other shocks of comparable magnitude, such as that in 2001 (Wang et al. 2001) following the very large transient event on the Sun in July 2000, this shock had no known association with solar events of the right magnitude, as the last series of large events on the Sun in solar cycle 23 took place in October–November 2003. The shock was followed by a MIR of 40 days duration, corresponding to a width of about 10 AU at the speed of the solar wind (∼450 km/s). There were increases in the magnetic field magnitude, solar wind density and solar wind temperature, all indicative of the dynamic processes resulting from interacting and coalescing component interaction regions during the solar wind transit from close to the Sun to close to the Termination Shock. Richardson et al. (2006b) concluded that the shock and the following MIR may have resulted from a piling up of stream interactions closer to Sun, as high speed streams started developing during the declining phase of solar cycle 23, or alternatively from a series of solar transients (flares and CMEs) that did not result in ICMEs observed in the inner heliosphere. A further alternative was also offered by Richardson et al. (2006b): the event may have been the result of the nascent

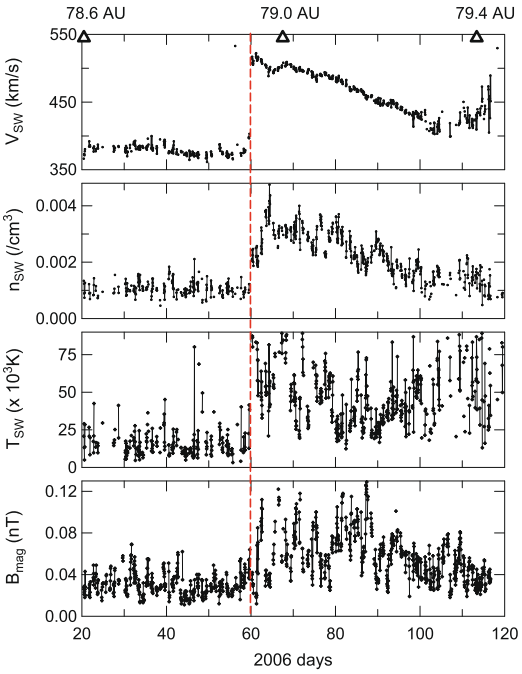

Fig. 25 Solar wind and magnetic field parameters measured at Voyager 2 at a heliocentric distance of ∼79 AU. A very large interplanetary shock was followed by a Merged Interaction region of duration ∼40 days, corresponding to about 8 to 10 AU in width. (Adapted from Richardson et al. 2006a)

stream interactions interacting during their evolution with the solar transients from September 2005. Although a unique example, this event—the very large shock, followed by the very wide MIR—represents a realization of evolving dynamic processes that make the outer heliosphere a generally poorly predictable medium.

5 Magnetic Field Fluctuations and Energetic Particle Transport

Fluctuations in the HMF are ubiquitous: there is a population of directional and magnitude fluctuations superimposed on the average Parker magnetic field throughout the heliosphere. Since the early works of Coleman (1968), it is well known that the power spectrum of magnetic field fluctuations generally follows a Kolmogorov spectrum with an approximately $-5/3$ exponent as a function of wavenumber. However, at small wavenumbers (corresponding to several hours in time for a stationary observer in the solar wind) the spectrum has an exponent ~ -1, and at high wavenumbers (above approximately the ion gyrofrequency) the spectrum is steeper, due to the other turbulent and/or dissipative processes. But the nature of the turbulence remains subject to ongoing research, due to the complexity of processes that involve the frequent presence of large amplitude Alfvén waves, as first identified by Belcher and Davis (1971). (For recent comprehensive reviews, see Goldstein and Roberts 1999; Bruno and Carbone 2005; Petrosyan et al. 2010 and references therein). The propagation of cosmic rays and energetic charged particles accelerated on the Sun and the heliosphere depends on the spatial and temporal characteristics of this fluctuating and turbulent medium. Early analysis of the propagation of energetic particles that involved scattering by small amplitude waves by Jokipii (1966) has led to the quasi-linear theory (QLT) of particle propagation that relates the energy spectrum of fluctuations in the magnetic field to the propagation coefficients of the energetic particles.

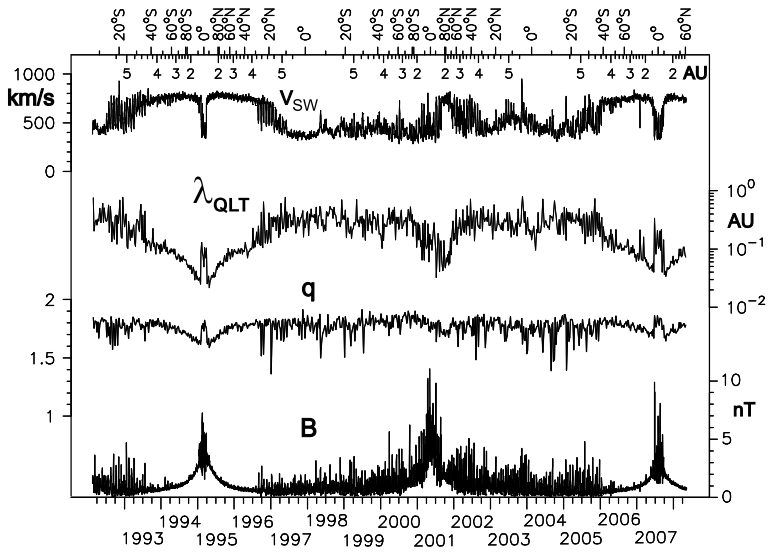

Fig. 26 Solar wind parameters and the mean free path of 1 MEV protons calculated from the magnetic field fluctuations observed along the Ulysses spacecraft trajectory from 1992 to 2008. From the top: solar wind speed, mean free path calculated using QLT, the spectral exponent of the power of the magnetic fluctuations, and the magnitude of the magnetic field. Along the top, the heliolatitude and the heliocentric distance of the observations is shown

With the increased understanding of the nature of fluctuations and magnetic turbulence, the original theory has been extended in different solar wind regimes and magnetic field configurations (see, e.g. Dröge 2000; Giacalone 2011, this issue, and references therein). Although QLT, using the observed magnetic field fluctuations to derive the transport coefficients of energetic particles, has been shown to yield a diffusion coefficient and a corresponding mean free path parallel to the magnetic field that are generally about an order of magnitude too small compared to experimentally determined values. However, the difference between QLT and experimentally fitted values of the mean free path are not consistently high, but cover a range of values characteristic of different energetic solar particle events (Wanner et al. 1993). Nevertheless, QLT remains a useful analytical framework for the study of cosmic ray propagation (see, e.g. He and Qin 2011). The experimental data were first summarised by Palmer (1982) and more recently reviewed by Giacalone (2011, this issue).

Given the exceptional coverage of the Ulysses mission over ∼18 years, covering the wide heliolatitude and heliocentric range already described in Sect. 1, it remains useful to derive the QLT mean free path over these parameter ranges. Preliminary results were published by Erdős et al. (1999) and Erdős and Balogh (2005); here we present the updated results, covering the whole of the out of ecliptic epoch, from 1992 to 2008, of the Ulysses mission. The results are summarised in Fig. 26. They show that the mean free path determined using QLT is, as previously found, significantly shorter than the experimentally determined values. However, there are interesting dependences that are associated with the nature of the solar wind. In the fast solar wind (at high heliolatitudes, from the polar coronal holes) the mean free path is significantly smaller (by close to an order of magnitude) than in the slow solar wind in the ecliptic. The radial dependence of the mean free path can be fitted with a power law, $\lambda_{QLT} \sim r^{1.3}$ (see Erdős and Balogh 2005) where r is the heliocentric distance in AU.

Once this radial dependence is removed from the results, the mean free path is independent of heliolatitude and only appears to depend on the origin (and speed) of the solar wind.

Solar wind turbulence has been shown to be fundamentally quasi-two dimensional, with a much smaller proportion of the fluctuation power in the "slab" turbulence which provides the effective power for scattering energetic particles (Bieber et al. 1996). The so-called "slab" fluctuations refer to Alfvénic fluctuations with wavevectors parallel to the magnetic field. However, the wavevectors of Alfvénic fluctuations have a range of directions and it has been found by Bieber et al. (1996) that only about 20% of the power in the magnetic fluctuations have wavevectors parallel to the magnetic field and the remaining 80%, the 2D component of the turbulence, have wavevectors that are approximately perpendicular to the magnetic field. The scattering power is thereby reduced, as the 2D fluctuations do not lead to the scattering of the propagating energetic particles and therefore the mean free path calculated is increased to provide a better match to the observations (Bieber et al. 1994). However, the original division between 2D and slab fluctuations identified by Bieber et al. (1996) may not be a general value, but will depend on the context in the solar wind, so that a significant qualitative difference between fast and slow wind is expected.

Even if the mean free path problem is in principle resolved by applying the quasi-2D composition of solar wind turbulence to calculating the transport parameters, the transport of energetic particles perpendicular to the magnetic field remains a problem. Indeed, while the transport of energetic particles perpendicular to the mean magnetic field direction is known to be significantly reduced when compared to parallel transport, there is evidence for greater than expected cross-field transport for energetic particles associated with Corotating Interaction regions (Intriligator et al. 2001). An important contributing phenomenon may well be the random mixing of magnetic field lines, although this is difficult to demonstrate from observations. Recent developments have included the analytical treatment of how both slab and 3D turbulence lead to perpendicular transport (Fraschetti and Jokipii 2011). Using the quasi-2D turbulence paradigm, Minnie et al. (2009) have explored the relationship between parallel and perpendicular transport and the respective roles of perpendicular scattering of particles and the random mixing of magnetic field lines and concluded that the two processes are inter-related and depend on scale sizes, turbulence regimes and particle energy. Perpendicular transport remains, nevertheless, a problem for both the interpretation of observations and the theoretical framework in which it can be best described.

6 Summary and Conclusions

The Heliospheric Magnetic Field is a key component of the heliospheric medium and the controlling active agent in the access and modulation of cosmic rays. Its general structure and three-dimensional topology is reasonably well understood, following the original model by Parker (1959). In the inner heliosphere, out to probably about 10 AU, the links between the solar corona and the Sun's open magnetic flux on the one hand, and the polarity, strength and average direction of the magnetic field are clear and generally, even in detail, well documented.

The dynamics of the heliospheric magnetic field are controlled by solar variability. Around solar minimum, the pattern of high speed solar wind streams and open magnetic field lines from the large polar coronal holes interacts, at its equatorial boundaries, with slow solar wind associated with the near equatorial streamer belt. The resulting interaction creates the well known pattern of Corotating Interaction Regions, the most prominent feature of the inner heliosphere around solar minimum activity. However, the dynamic evolution of

these well ordered streams and interacting shock waves leads to a significant breakup of the order and results in more chaotic conditions in the outer heliosphere, in fact probably outwards from 10 to 20 AU. Although there are no observations at high heliolatitudes in the outer heliosphere, it is expected that the relatively uniform solar wind flow leads to a smaller degree of large-amplitude disorder in low solar activity years.

Solar variability becomes more pronounced, on a broader range of timescales, around solar maximum. Generally, solar transients, CMEs, dominate at all heliolatitudes, leading to complex patterns of interactions already in the inner heliosphere. The resulting single or multiple ICMEs produce a train of transient enhancements in the heliospheric magnetic field, usually richly endowed with shock waves, large amplitude deflections and a range of compressive features. This already complex pattern evolves throughout the heliosphere, resulting in chaotic structures, although, as discussed above, occasionally evidently capable of coalescing into large-scale and large-amplitude fluctuating structures. The very large transients due to the most energetic solar eruptions cause the large Forbush decreases in cosmic rays, through the formation of Merged Interaction Regions, of which the largest may well be global in the sense of enclosing the inner part of the heliosphere a shell of much enhanced magnetic fields.

Cosmic ray propagation through the heliosphere remains a very active research topic in which understanding of large-scale structures needs to be combined with an understanding of the fluctuations in the magnetic field at all scales. The description of heliospheric fluctuations in terms of turbulent processes has made some progress over the past three decades, although beyond the evidence that the description of turbulence needs to be anisotropic and three dimensional, the models of energetic particle transport remain controversial. In particular, the two long-standing questions of why transport parallel to the magnetic field is easier, with longer mean free paths, than calculated and why there is apparently, at least in some important circumstances, much more effective transport perpendicular to the magnetic field have not been satisfactorily answered in general. The 2D nature of the turbulence may resolve at least the first question, eventually quantitatively. Perpendicular transport is more challenging as it is more difficult to assess experimentally and would require a more detailed knowledge of the magnetic field structure and its fluctuations in three dimensions.

It is clear that the lack of observations has been and is likely to remain a seriously limiting factor in understanding all the important aspects of the heliospheric magnetic field. The inner heliosphere has been and will remain relatively well served by observational platforms, particularly close to 1 AU and the ecliptic, in the service of monitoring space weather conditions. The outer heliosphere, in fact anything beyond a few AU will now remain unexplored beyond what we know from the Pioneer and, most importantly, from the Voyager missions. The remarkable journey of the two Voyager spacecraft have provided some vital information on the outer heliosphere (and now on the heliosheath beyond the Termination Shock), but these are only two, single point sets of observations, with limited instrumental capability, due to inherent difficulties of achieving the required sensitivities and even reliability after more than 40 years in space. The much more comprehensively equipped Ulysses and ACE spacecraft (and now the two STEREO spacecraft) have emphasized the need for a comprehensive coverage of particle and field instruments, in particular for the measurement of the plasma composition and the ionic charge composition, as well as continuous time coverage, to make real progress in the future. Theoretical models will be able to progress to model the dynamics of the heliospheric medium, but the necessary observational tests will continue to rely on already acquired data sets. The importance of these data sets for the future of heliospheric research cannot be overemphasized.

Acknowledgements The authors are grateful for the ready availability of the key data sets from all the important heliospheric spacecraft. Their work in writing this review has also been greatly facilitated by the equally ready availability of journals, as witnessed by the extensive (and still not exhaustive) bibliography listed. AB happily acknowledges his association with the directors and staff of the International Space Science Institute in Bern, Switzerland who have provided a wonderful work environment. Furthermore, AB also thanks his colleagues in Imperial College and in the Ulysses science team for much illuminating education on magnetic fields in the heliosphere. Very special thanks are due to Dr Ed Smith, of the Jet Propulsion Laboratory, Pasadena, California, for his friendship and his advice on all aspects of magnetic fields in space.

References

A. Balogh, Magnetic fields in the heliosphere at solar minimum and solar maximum, in *Proceedings of the Second Granada Workshop, "The Evolving Sun and its Influence on Planetary Environments"*, ed. by B. Montesinos, A. Gimenez, E.F. Guinan. ASP Conf. Series, vol. 269 (2002), pp. 37–72

A. Balogh, J.R. Jokipii, The heliospheric magnetic field and its extension to the inner heliosheath. Space Sci. Rev. **143**, 85–110 (2009)

A. Balogh, G. Erdös, R.J. Forsyth, E.J. Smith, The evolution of the interplanetary sector structure in 1992. Geophys. Res. Lett. **20**, 2331–2334 (1993)

A. Balogh, J.A. Gonzalez-Esparza, R.J. Forsyth, M.E. Burton, B.E. Goldstein, E.J. Smith, Interplanetary shock waves: Ulysses observations in and out of the ecliptic plane. Space Sci. Rev. **72**, 171–180 (1995)

S.J. Bame, B.E. Goldstein, J.T. Gosling, J.W. Harvey, D.J. McComas, M. Neugebauer, J.L. Phillips, Ulysses observations of a recurrent high speed stream and the heliomagnetic streamer belt. Geophys. Res. Lett. **20**, 2323–2326 (1993)

K.W. Behannon, Heliocentric distance dependence of the interplanetary magnetic field. Rev. Geophys. Space Phys. **16**, 125–145 (1978)

J.W. Belcher, L. Davis Jr., Large-amplitude Alfvén waves in the interplanetary medium, 2. J. Geophys. Res. **76**, 3534–3563 (1971)

J.W. Belcher, A.J. Lazarus, R.L. McNutt Jr., G.S. Gordon Jr., Large-scale density structures in the outer heliosphere. Adv. Space Res. **13**, 41–46 (1993)

J.W. Bieber, W.H. Matthaeus, C.W. Smith, W. Wanner, M.-B. Kallenrode, G. Wibberenz, Proton and electron mean free paths: the Palmer consensus revisited. Astrophys. J. **420**, 294–306 (1994)

J.W. Bieber, W. Wanner, W.H. Matthaeus, Dominant two-dimensional solar wind turbulence with implications for cosmic ray transport. J. Geophys. Res. **101**, 2511–2522 (1996)

J.E. Borovsky, On the variations of the solar wind magnetic field about the Parker spiral direction. J. Geophys. Res. **115**, A09101 (2010). doi:10.1029/2009JA015040

R. Bruno, V. Carbone, The solar wind as a turbulence laboratory. Living Rev. Sol. Phys. **2** (2005). http://www.livingreviews.org/lrsp-2005-4

L.F. Burlaga, Magnetic clouds and force-free fields with constant alpha. J. Geophys. Res. **93**, 7217–7224 (1988)

L.F. Burlaga, N.F. Ness, Merged interaction regions and large-scale magnetic field fluctuations during 1991: Voyager 2 observations. J. Geophys. Res. **99**, 19,341–19,350 (1994)

L.F. Burlaga, N.F. Ness, Magnetic fields in the distant heliosphere approaching solar minimum: Voyager 1 and 2 observations during 1994. J. Geophys. Res. **101**, 13473–13481 (1996)

L.F. Burlaga, E. Sittler, F. Mariani, R. Schwenn, Magnetic loop behind an interplanetary shock—Voyager, Helios, and IMP 8 observations. J. Geophys. Res. **86**, 6673–6684 (1981)

L.F. Burlaga, L. Klein, N.R. Sheeley Jr., D.J. Michels, R.A. Howard, M.J. Koomen, R. Schwenn, H. Rosenbauer, A magnetic cloud and a coronal mass ejection. Geophys. Res. Lett. **9**, 1317–1320 (1982)

L.F. Burlaga, R. Schwenn, H. Rosenbauer, Dynamical evolution of interplanetary magnetic fields and flows-between 0.3 AU and 8.5 AU: Entrainment. Geophys. Res. Lett. **10**, 413–416 (1983)

L.F. Burlaga, W.H. Mish, Y.C. Whang, Coalescence of recurrent streams of different sizes and amplitudes. J. Geophys. Res. **95**, 4247–4255 (1990)

L.F. Burlaga, N.F. Ness, J.W. Belcher, Radial evolution of corotating merged interaction regions and flows between ∼14 AU and ∼43 AU. J. Geophys. Res. **102**, 4661–4671 (1997)

L.F. Burlaga, N.F. Ness, J.D. Richardson, R.P. Lepping, The Bastille day shock and merged interaction region at 63 AU: Voyager 2 observations. Sol. Phys. **204**, 399–411 (2001)

L.F. Burlaga, D. Berdichevsky, N. Gopalswamy, R. Lepping, T. Zurbuchen, Merged interaction regions at 1 AU. J. Geophys. Res. **108**(A12), 1425 (2003a). doi:10.1029/2003JA010088

L.F. Burlaga, N.F. Ness, J.D. Richardson, Sectors in the distant heliosphere: Voyager 1 and 2 observations from 1999 through 2002 between 57 and 83 AU. J. Geophys. Res. **108**(A10), 8028 (2003b). doi:10.1029/2003JA009870

L.F. Burlaga, C. Wang, J.D. Richardson, N.F. Ness, Evolution of magnetic fields in corotating interaction regions from 1 to 95 AU: order to chaos. Astrophys. J. **590**, 554–566 (2003c)
L.F. Burlaga, N.F. Ness, F.B. McDonald, J.D. Richardson, C. Wang, Voyager 1 and 2 observations of magnetic fields and associated cosmic-ray variations from 2000 through 2001: 60–87 AU. Astrophys. J. **582**, 540–549 (2003d)
H.V. Cane, I.G. Richardson, Interplanetary coronal mass ejections in the near-Earth solar wind during 1996–2002. J. Geophys. Res. **108**(A4), 1156 (2003). doi:10.1029/2002JA009817
P.J. Cargill, J.M. Schmidt, Modelling interplanetary CMEs using magnetohydrodynamic simulations. Ann. Geophys. **20**, 879–890 (2002)
M.L. Cartwright, M.B. Moldwin, Comparison of small-scale flux rope magnetic properties to large-scale magnetic clouds: Evidence for reconnection across the HCS? J. Geophys. Res. **113**, A09105 (2008). doi:10.1029/2008JA013389
M.L. Cartwright, M.B. Moldwin, Heliospheric evolution of solar wind small-scale magnetic flux ropes. J. Geophys. Res. **115**, A08102 (2010). doi:10.1029/2009JA014271
P.J. Coleman Jr., Turbulence, viscosity and dissipation in the solar wind plasma. Astrophys. J. **153**, 371–388 (1968)
P. Démoulin, S. Dasso, Magnetic cloud models with bent and oblate cross-section boundaries. Astron. Astrophys. **507**, 969–980 (2009)
W. Dröge, Particle scattering by magnetic fields. Space Sci. Rev. **93**, 121–151 (2000)
G. Erdõs, A. Balogh, The symmetry of the heliospheric current sheet as observed by Ulysses during the fast latitude scan. Geophys. Res. Lett. **25**, 245–248 (1998)
G. Erdős, A. Balogh, In situ observations of magnetic field fluctuations. Adv. Space Res. **35**, 625–635 (2005)
G. Erdõs, A. Balogh, North-south asymmetry of the location of the heliospheric current sheet revisited. J. Geophys. Res. **115**, A01105 (2010). doi:10.1029/2009JA014620
G. Erdős, A. Balogh, J. Kóta, Scattering mean free path of energetic protons in the heliosphere, in *Proceedings 26th International Cosmic Ray Conference*, Salt Lake City, 1999, vol. 6 (1999), pp. 316–319
H.Q. Feng, D.J. Wu, C.C. Lin, J.K. Chao, L.C. Lee, L.H. Lyu, Interplanetary small- and intermediate-sized magnetic flux ropes during 1995–2005. J. Geophys. Res. **113**, A12105 (2008). doi:10.1029/2008JA013103
L.A. Fisk, Motion of the footpoints of heliospheric magnetic field lines at the Sun: implications for recurrent energetic particle events at high heliographic latitudes. J. Geophys. Res. **101**, 15547–15554 (1996)
T. Forbes, A review on the genesis of coronal mass ejections. J. Geophys. Res. **105**, 23153–23166 (2000)
T. Forbes, J.A. Linker, J. Chen, C. Cid, J. Kóta, M.A. Lee, G. Mann, Z. Mikic, M.S. Potgieter, J.M. Schmidt, et al., CME theory and models—report of working group D. Space Sci. Rev. **123**, 251–302 (2006)
R.J. Forsyth, A. Balogh, T.S. Horbury, G. Erdos, E.J. Smith, M.E. Burton, The heliospheric magnetic field at solar minimum: Ulysses observations from pole to pole. Astron. Astrophys. **316**, 287–295 (1996)
R.J. Forsyth, A. Balogh, E.J. Smith, The underlying direction of the heliospheric magnetic field through the Ulysses first orbit. J. Geophys. Res. **107**(A11), 1405 (2002). doi:10.1029/2001JA005056
F. Fraschetti, J.R. Jokipii, Time-dependent perpendicular transport of fast charged particles in a turbulent magnetic field. Astrophys. J. **734**(2), 83 (2011). doi:10.1088/0004-637X/734/2/83
P.R. Gazis, A large-scale survey of corotating interaction regions and their successors in the outer heliosphere. J. Geophys. Res. **105**, 19–23 (2000)
J. Geiss, G. Gloeckler, R. von Steiger, Origin of the solar wind from composition data. Space Sci. Rev. **72**, 49–60 (1995)
J. Giacalone, Cosmic-ray transport and interaction with shocks. Space Sci. Rev. (2011, this issue). doi:10.1007/s11214-011-9763-2
M.L. Goldstein, D.A. Roberts, Magnetohydrodynamic turbulence in the solar wind. Phys. Plasmas **6**, 4154–4160 (1999)
J.A. Gonzalez-Esparza, E.J. Smith, Solar cycle dependence of solar wind dynamics: Pioneer, Voyager and Ulysses from 1 to 5 AU. J. Geophys. Res. **101**, 24359–24371 (1996)
J.T. Gosling, Coronal mass ejections and magnetic flux ropes in interplanetary space, in *Physics of Magnetic Flux Ropes*, ed. by C.T. Russell, E.R. Priest, L.C. Lee. Geophysical Monograph, vol. 58 (American Geophysical Union, Washington, 1990), pp. 343–364
J.T. Gosling, V.J. Pizzo, Formation and evolution of corotating interaction regions and their three dimensional structure. Space Sci. Rev. **89**, 21–52 (1999)
J.T. Gosling, R.M. Skoug, On the origin of radial magnetic fields in the heliosphere. J. Geophys. Res. **107**(A10), 1327 (2002). doi:10.1029/2002JA009434
J.T. Gosling, A.J. Hundhausen, S.J. Bame, Solar wind stream evolution at large heliocentric distances: Experimental demonstration and the test of a model. J. Geophys. Res. **81**, 2111–2122 (1976)
J.T. Gosling, J.R. Asbridge, S.J. Bame, W.C. Feldman, Solar wind stream interfaces. J. Geophys. Res. **83**, 1401–1412 (1978)

H.-Q. He, G. Qin, A simple analytical method to determine solar energetic particles' mean free path. Astrophys. J. **730**(1), 46 (2011). doi:10.1088/0004-637X/730/1/46
J.T. Hoeksema, Extending the Sun's magnetic field through the three-dimensional heliosphere. Adv. Space Res. **9**, 141–152 (1989)
H.S. Hudson, J.-L. Bougeret, J. Burkepile, Coronal mass ejections: Overview of observations. Space Sci. Rev. **123**, 13–30 (2006)
A.J. Hundhausen, Evolution of large-scale solar wind structures beyond 1 AU. J. Geophys. Res. **78**, 2035–2042 (1973)
A.J. Hundhausen, Sizes and locations of coronal mass ejections: SMM observations from 1980 and 1984–1989. J. Geophys. Res. **98**, 13177–13200 (1993)
D.S. Intriligator, J.R. Jokipii, T.S. Horbury, J.M. Intriligator, R.J. Forsyth, H. Kunow, G. Wibberenz, J.T. Gosling, Processes associated with particle transport in corotating interaction regions and near stream interfaces. J. Geophys. Res. **106**, 10625–10634 (2001)
L. Jian, C.T. Russell, J.G. Luhmann, R.M. Skoug, Properties of stream interaction regions at one AU during 1995–2004. Sol. Phys. **239**, 337–392 (2006)
L.K. Jian, C.T. Russell, J.G. Luhmann, A.B. Galvin, P.J. MacNeice, Multi-spacecraft observations: Stream interactions and associated structures. Sol. Phys. **259**, 345–360 (2009)
J.R. Jokipii, Cosmic-ray propagation. I. Charged particles in a random magnetic field. Astrophys. J. **146**, 480–487 (1966)
J.R. Jokipii, J. Kóta, The polar heliospheric magnetic field. Geophys. Res. Lett. **16**, 1–4 (1989)
G.H. Jones, A. Balogh, R.J. Forsyth, Radial heliospheric magnetic fields detected by Ulysses. Geophys. Res. Lett. **25**, 3109–3112 (1998)
G.H. Jones, A. Balogh, E.J. Smith, Solar magnetic field reversal as seen at Ulysses. Geophys. Res. Lett. **30**(19), 8028 (2003). doi:10.1029/2003GL017204
S.W. Kahler, S. Krucker, A. Szabo, Solar energetic electron probes of magnetic cloud field line lengths. J. Geophys. Res. **116**, A01104 (2011). doi:10.1029/2010JA015328
L.W. Klein, L.F. Burlaga, Interplanetary magnetic clouds at 1 AU. J. Geophys. Res. **87**, 613–624 (1982)
H. Kunow, N.U. Crooker, J.A. Linker, R. Schwenn, R. Von Steiger (eds.), *Coronal Mass Ejections*. Space Science Series of ISSI, vol. 21. Reprinted from Space Science Reviews Journal, vol. 123/1–4 (2006)
R.P. Lepping, J.A. Jones, L.F. Burlaga, Magnetic field structure of interplanetary magnetic clouds at 1 AU. J. Geophys. Res. **95**, 11957–11965 (1990)
R.P. Lepping, D.B. Berdichevsky, L.F. Burlaga, A.J. Lazarus, J. Kasper, M.D. Desch, C.-C. Wu, D.V. Reames, H.J. Singer, C.W. Smith, K.L. Ackerson, The Bastille day magnetic clouds and upstream shocks: near-Earth interplanetary observations. Sol. Phys. **204**, 287–305 (2001)
R.P. Lepping, C.-C. Wu, D.B. Berdichevsky, A. Szabo, Magnetic clouds at/near the 2007–2009 solar minimum: Frequency of occurrence and some unusual properties. Sol. Phys. (2011). doi:10.1007/s11207-010-9646-9
S.T. Lepri, T.H. Zurbuchen, L.A. Fisk, I.G. Richardson, H.V. Cane, G. Gloeckler, Iron charge distribution as an identifier of interplanetary coronal mass ejections. J. Geophys. Res. **106**, 29231–29238 (2001)
F.B. McDonald, A. Barnes, L.F. Burlaga, P. Gazis, J. Mihalov, R.S. Selesnick, Effects of the intense solar activity of March/June 1991 observed in the outer heliosphere. J. Geophys. Res. **99**, 14705–14715 (1994)
F.B. McDonald, L.F. Burlaga, A.C. Cummings, B.C. Heikkila, N. Lal, N.F. Ness, E.C. Stone, J.D. Richardson, W.R. Webber, The July 14th, 2000 "Bastille Day" solar event as observed by Voyagers 1 and 2 in the distant heliosphere, in *Proc. 27th Internat. Cosmic Ray Conf.* Copernicus Gesellschaft (2001), pp. 3637–3640
J. Minnie, W.H. Matthaeus, J.W. Bieber, D. Ruffolo, R.A. Burger, When do particles follow field lines? J. Geophys. Res., **114**, A01102 (2009). doi:10.1029/2008JA013349
M.B. Moldwin, J.L. Phillips, J.T. Gosling, E.E. Scime, D.J. McComas, S.J. Bame, A. Balogh, R.J. Forsyth, Ulysses observations of a noncoronal mass ejection flux rope: Evidence of interplanetary magnetic reconnection. J. Geophys. Res. **100**, 19903–19910 (1995). doi:10.1029/95JA01123
C. Möstl, C.J. Farrugia, H.K. Biernat, M. Leitner, E.K.J. Kilpua, A.B. Galvin, J.G. Luhmann, Optimized Grad–Shafranov reconstruction of a magnetic cloud using STEREO-Wind observations. Sol. Phys. **256**, 427–441 (2009)
D. Odstrcil, P. Riley, J.A. Linker, R. Lionello, Z. Mikic, V.J. Pizzo, 3-D simulations of ICMEs by coupled coronal and heliospheric models, in *Solar Variability as an Input to the Earth's Environment*. ESA SP, vol. 535 (European Space Agency, Noordwijk, 2003), pp. 541–546
I.D. Palmer, Transport coefficients of low-energy cosmic rays in interplanetary space. Rev. Geophys. Space Phys. **20**, 335–351 (1982)
E.N. Parker, Extension of the solar corona into interplanetary space. J. Geophys. Res. **64**, 1675–1681 (1959)
K.I. Paularena, C. Wang, R. von Steiger, B. Heber, An ICME observed by Voyager 2 at 58 AU and by Ulysses at 5 AU. Geophys. Res. Lett. **28**, 2755–2758 (2001)

A. Petrosyan, A. Balogh, M.L. Goldstein, J. Léorat, E. Marsch, K. Petrovay, B. Roberts, R. von Steiger, J.-C. Vial, Turbulence in the solar atmosphere and solar wind. Space Sci. Rev. **156**, 135–238 (2010)
V.J. Pizzo, Global, quasi-steady dynamics of the distant solar wind 2. Deformation of the heliospheric current sheet. J. Geophys. Res. **99**, 4185–4191 (1994)
A. Rees, R.J. Forsyth, Two examples of magnetic clouds with double rotations observed by the Ulysses spacecraft. Geophys. Res. Lett. **31**, L06804 (2004). doi:10.1029/2003GL018330
J.D. Richardson, Y. Liu, C. Wang, D.J. McComas, E.C. Stone, A.C. Cummings, L.F. Burlaga, M.H. Acuna, N.F. Ness, Source and consequences of a large shock near 79 AU. Geophys. Res. Lett. **33**, L23107 (2006a). doi:10.1029/2006GL027983
J.D. Richardson, Y. Liu, C. Wang, L.F. Burlaga, ICMEs at very large distances. Adv. Space Res. **38**, 528–534 (2006b)
I.G. Richardson, H.V. Cane, Near-Earth interplanetary coronal mass ejections during solar cycle 23 (1996–2009): Catalog and summary of properties. Sol. Phys. **264**, 189–237 (2010)
P. Riley, N.U. Crooker, Kinematic treatment of coronal mass ejection evolution in the solar wind. Astrophys. J. **600**, 1035–1042 (2004)
P. Riley, J.A. Linker, Z. Mikic, Modeling the heliospheric current sheet: Solar cycle variations. J. Geophys. Res. **107 A7**, 1136 (2002). doi:10.1029/2001JA000299
P. Riley, J.A. Linker, R. Lionello, Z. Mikić, D. Odstrcil, M.A. Hidalgo, C. Cid, Q. Hu, R.P. Lepping, B.J. Lynch, A. Rees, Fitting flux ropes to a global MHD solution: A comparison of techniques. J. Atmos. Sol.-Terr. Phys. **66**, 1321–1331 (2004)
P. Riley, J.A. Linker, Z. Mikic, D. Odstrcil, Modeling interplanetary coronal mass ejections. Adv. Space Res. **38**, 535–546 (2006a)
P. Riley, C. Schatzman, H.V. Cane, I.G. Richardson, N. Gopalswamy, On the rates of coronal mass ejections: Remote solar and in situ observations. Astrophys. J. **647**, 648–653 (2006b)
E. Robbrecht, D. Berghmans, R.A.M. Van der Linden, Automated LASCO CME catalog for solar cycle 23: Are CMEs scale invariant? Astrophys. J. **691**, 1222–1234 (2009)
M. Schulz, Interplanetary sector structure and the heliomagnetic equator. Astrophys. Space Sci. **24**, 371–383 (1973)
R. Schwenn, Heliospheric 3D structure and CME propagation as seen from SOHO: Recent lessons for space weather predictions. Adv. Space Res. **26**, 43–53 (2000)
J.A. Simpson, M. Zhang, S. Bame, A solar polar north-south asymmetry for cosmic-ray propagation in the heliosphere: The Ulysses pole-to-pole rapid transit. Astrophys. J. **465**, L69–L72 (1996)
E.J. Smith, Interplanetary magnetic field over two solar cycles and out to 20 AU. Adv. Space Res. **9**, 159–169 (1989)
E.J. Smith, The heliospheric current sheet. J. Geophys. Res. **106**, 15819–15831 (2001)
E.J. Smith, The global heliospheric magnetic field, in *The Heliosphere Through the Solar Activity Cycle*, ed. by A. Balogh, L.J. Lanzerotti, S.T. Suess (Springer, Chichester, 2007), pp. 79–150
E.J. Smith, J.H. Wolfe, Observations of interaction regions and corotating shocks between one and five AU: Pioneers 10 and 11. Geophys. Res. Lett. **3**, 137–140 (1976)
E.J. Smith, A. Balogh, Ulysses observations of the radial magnetic field. Geophys. Res. Lett. **22**, 3317–3320 (1995)
E.J. Smith, M. Neugebauer, A. Balogh, S.J. Bame, G. Erdős, R.J. Forsyth, B.E. Goldstein, J.L. Phillips, B.T. Tsurutani, Disappearance of the heliospheric sector structure at Ulysses. Geophys. Res. Lett. **20**, 2327–2330 (1993)
B.U.Ö. Sonnerup, H. Hasegawa, W.-L. Teh, L.-N. Hau, Grad–Shafranov reconstruction: An overview. J. Geophys. Res. **111**, A09204 (2006). doi:10.1029/2006JA011717
B.T. Thomas, E.J. Smith, The Parker spiral configuration of the interplanetary magnetic field between 1 and 8.5 AU. J. Geophys. Res. **85**, 6861–6867 (1980)
B.T. Thomas, E.J. Smith, The structure and dynamics of the heliospheric current sheet. J. Geophys. Res. **86**, 11105–11110 (1981)
M. Vandas, E.P. Romashets, S. Watari, A. Geranios, E. Antoniadou, O. Zacharopoulou, Comparison of force-free flux rope models with observations of magnetic clouds. Adv. Space Res. **38**, 441–446 (2006)
R. von Steiger, T.H. Zurbuchen, Composition signatures of interplanetary coronal mass ejections, in *Solar Variability as an Input to the Earth's Environment*. ESA SP, vol. 535 (European Space Agency, Noordwijk, 2003), pp. 835–840
R. von Steiger, J.D. Richardson, ICMEs in the outer heliosphere and at high latitudes: an introduction. Space Sci. Rev. **123**, 111–126 (2006)
A. Vourlidas, R.A. Howard, E. Esfandiari, S. Patsourakos, S. Yashiro, G. Michalek, Comprehensive analysis of coronal mass ejections mass and energy properties over a full solar cycle. Astrophys. J. **722**, 1522–1538 (2010)

C. Wang, J.D. Richardson, Interplanetary coronal mass ejections observed by Voyager 2 between 1 and 30 AU. J. Geophys. Res. **109**, A06104 (2004). doi:10.1029/2004JA010379
C. Wang, J.D. Richardson, Dynamic processes in the outer heliosphere: Voyager observations and models. Adv. Space Phys. **35**, 2102–2105 (2005)
C. Wang, J.D. Richardson, L.F. Burlaga, Propagation of the Bastille Day 2000 CME shock in the outer heliosphere. Sol. Phys. **204**, 411–421 (2001)
C. Wang, J.D. Richardson, L.F. Burlaga, N.F. Ness, On radial heliospheric magnetic fields: Voyager 2 observation and model. J. Geophys. Res. **108**(A5), 1205 (2003). doi:10.1029/2002JA009809
C. Wang, D. Du, J.D. Richardson, Characteristics of the interplanetary coronal mass ejections in the heliosphere between 0.3 and 5.4 AU. J. Geophys. Res. **110**, A10107 (2005). doi:10.1029/2005JA011198
Y.-M. Wang, Coronal holes and open magnetic flux. Space Sci. Rev. **144**, 383–399 (2009)
Y.-M. Wang, N.R. Sheeley Jr., On potential field models of the solar corona. Astrophys. J. **392**, 310–319 (1992)
Y.-M. Wang, N.R. Sheeley, Solar implications of Ulysses interplanetary field measurements. Astrophys. J. **447**, L143–L146 (1995)
Y.-M. Wang, N.R. Sheeley, On the topological evolution of the coronal magnetic field during the solar cycle. Astrophys. J. **599**, 1404–1417 (2003)
Y.-M. Wang, N.R. Sheeley Jr., Sources of the solar wind at Ulysses during 1990–2006. Astrophys. J. **653**, 708–718 (2006)
Y.-M. Wang, N.R. Sheeley Jr., M.D. Andrews, Polarity reversal of the solar magnetic field during cycle 23. J. Geophys. Res. **107**(A12), 1465 (2002a). doi:10.1029/2002JA009463
Y.M. Wang, S. Wang, P.Z. Ye, Multiple magnetic clouds in interplanetary space. Sol. Phys. **211**, 333–344 (2002b)
Y.-M. Wang, E. Robbrecht, N.R. Sheeley, On the weakening of the polar magnetic fields during solar cycle 23. Astrophys. J. **707**, 1372–1386 (2009)
W. Wanner, M.-B. Kallenrode, W. Dröge, G. Wibberenz, Solar energetic proton mean free paths. Adv. Space Res. **13**, 359–362 (1993)
Y.C. Whang, Shock interactions in the outer heliosphere. Space Sci. Rev. **57**, 339–388 (1991)
Y.C. Whang, L.F. Burlaga, Evolution and interaction of interplanetary shocks. J. Geophys. Res. **90**, 10765–10778 (1985)
Y.C. Whang, L.F. Burlaga, Evolution of recurrent solar wind structures between 14 AU and the termination shock. J. Geophys. Res. **93**, 5446–5460 (1988)
Y.C. Whang, L.F. Burlaga, N.F. Ness, C.W. Smith, The Bastille day shocks and merged interaction region. Sol. Phys. **204**, 255–265 (2001)
J.M. Wilcox, N.F. Ness, Quasi-stationary corotating structure in the interplanetary medium. J. Geophys. Res. **70**, 5793–5805 (1965)
R.F. Wimmer-Schweingruber, N.U. Crooker, A. Balogh, V. Bothmer, R.J. Forsyth et al., Understanding interplanetary coronal mass ejection signatures. Space Sci. Rev. **123**, 177–216 (2006)
C.C. Wu, R.P. Lepping, Statistical comparison of magnetic clouds with interplanetary coronal mass ejections for solar cycle 23. Sol. Phys. **269**, 141–153 (2011)
X. Zhou, E.J. Smith, Solar cycle variations of heliospheric magnetic flux. J. Geophys. Res. **114**, A03106 (2009). doi:10.1029/2008JA013421
B. Zieger, K.C. Hansen, Statistical validation of a solar wind propagation model from 1 to 10 AU. J. Geophys. Res. **113**, A08107 (2008). doi:10.1029/2008JA013046
T. Zurbuchen, A new view of the coupling of the Sun and the heliosphere. Annu. Rev. Astron. Astrophys. **45**, 297–338 (2007)
T.H. Zurbuchen, I.G. Richardson, In-situ solar wind and magnetic field signatures of interplanetary coronal mass ejections. Space Sci. Rev. **123**, 31–43 (2006)